Master's Thesis

Microwave materials characterization using waveguides and coaxial probe

By

Christos Tsipogiannis

Department of Electrical and Information Technology
Faculty of Engineering, LTH, Lund University
SE-221 00 Lund, Sweden

to Alexandra and my family

στην Αλεξάνδρα και στην οικογένειά μου

"*Εν οίδα, ότι ουδέν οίδα*"

Σωκράτης

"*One I know, that I know nothing*"

Socrates

"*Γηράσκω αεί διδασκόμενος*"

Σόλων

"*As I age I always learn*"

Solon

Abstract

The complex permittivities of some liquid and solid samples have been measured using a reflection coaxial method in the first part of this thesis. The coaxial probe was modeled as an antenna and a calibration procedure with four standards was used. The complex permittivities and permeabilities of epoxy samples were determined using reflection and transmission data from a measurement using a filled rectangular waveguide in the second part of the thesis. This determination was based on data from measurements, simulations and mathematical calculations and evaluated with the Nicolson-Ross-Weir algorithm. Some Comsol Multiphysics models and data from partially filled waveguides are also presented.

Acknowledgments

Contents

1. Introduction

With the term *microwaves* the electromagnetic waves with wavelength from 1 cm to 1 m are commonly known. These wavelengths correspond to the frequency range from 300 MHz (for 1 m wavelength) to 30 GHz (for 1 cm wavelength). This range covers the Ultrahigh Frequency (UHF) and Superhigh Frequency (SHF) bands [Collin 2001, pp. 1-2].

Some typical services in these frequencies are Television, satellite communications, radiosondes, surveillance radars, navigation aid, airborne radars, microwave communication links, common-carrier land mobile communications, radar astronomy, Bluetooth and Radio Frequency Identification (RFID). Also microwave components are used in microwave ovens and radio telescopes [Collin 2001, pp. 2-6].

In all these applications microwave materials have been used. The development of these materials and the study of their properties at microwave frequencies are very active areas in materials science, solid-state physics and electrical and electronic engineering. The development of high-frequency circuits require complete understanding of the properties of materials operating at microwave frequencies [Waser 2003]. Therefore a very important area in microwave electronics for many industries and scientists is the *characterization* of materials properties [Chen, Ong, Neo, Varadan, Varadan 2004, p. xi]. The term *electromagnetic characterization* or simply *characterization* refers to the full knowledge of the electromagnetic parameters -complex permittivity and permeability- of a material as functions against frequency.

Beyond the academic importance of the study of the electromagnetic properties at these frequencies [Solymar and Walsh 1998, Kittel 1997, Von Hippel 1995a,b, Jiles 1994], in microwave engineering the accurate constitutive properties are demanded [Ramo, Whinnery, Van Duzer 1994].

Since the early 1950's the characterization of materials properties at microwave frequencies has introduced and used. The ability of tailoring the properties of composite materials has been very important for the design and development of radar absorbing materials since World War II [Knott, Shaeffer, Tuley 2004]. Huge steps have been made during the last decades and many methods and techniques have been developed. As the clock speeds of electronic devices are approaching microwave frequencies the development of electronic circuits requires precise knowledge of the properties of materials, such as permittivity and permeability. Special materials are needed to ensure Electromagnetic Compatibility (EMC) since the Electromagnetic Interference must be taken into consideration in the design of circuit and packaging [Montrose 1999]. Nowadays the study of electromagnetic materials is also helpful for agriculture, food engineering, bioengineering, medical treatments [Thuery 1992], and in monitoring the fabrication procedure and nondestructive testing of samples and products [Zoughi 2000, Nyfors and Vainikainen 1989].

This Thesis is dedicated to two kinds of methods of materials characterization, reflection and transmission/reflection. The goals of this Thesis are to use two experimental methods and some simulations to derive the properties of some materials, to highlight the advantages and disadvantages of one reflection and one transmission reflection method and to use the Comsol Multiphysics program to investigate its possibilities to produce scattering parameters similar to the measured ones -for both filled and partially filled waveguides. Another goal is to check the evaluation of the scattering parameters from a partially filled waveguide with the Nicolson Ross Weir algorithm and also to implement some algorithms and a calibration procedure with the Matlab software.

This short chapter is a general Introduction to the reader. In Chapter 2 the theoretical principals are being presented so that any person who knows the fundamental of Electromagnetism can read this Thesis. Chapters 3 and 4 are presenting the methods, models and algorithms that have been used. In Chapter 5 the experiments, the simulations and their results are being quoted. The conclusions are summarized in Chapter 6 and in Chapter 7 some future work is being suggested. At last in Chapter 8 all the references are being given.

2. Theoretical Background

2.1 Electromagnetic Materials

Materials are primarily divided in *insulators*, *semiconductors* and *conductors* regarding the number of the free electrons of their atoms. According to the responses of the magnetic moments of their atoms to an external magnetic field, materials can be classified into *diamagnetic*, *paramagnetic* and *ordered magnetic materials*. Materials that are negligibly affected by magnetic fields are known as *nonmagnetic*. Usually is assumed that *insulators* are *nonmagnetic* and they are called *dielectrics*.

The electric and magnetic behavior of a low-conductivity material is determined by two complex parameters, *permittivity (ε)* and *permeability (μ)*

$$\varepsilon = \varepsilon' - j\varepsilon'' \tag{2.1}$$

$$\mu = \mu' - j\mu'' \tag{2.2}$$

Permittivity describes the interaction of a material with the electric field applied on it and respectively permeability describes the interaction of a material with the magnetic field applied on it. The electric and magnetic fields interact with materials in two ways, *energy storage* and *energy dissipation*.

Energy storage describes the lossless portion of the exchange of energy between the field and the material. Energy dissipation occurs when electromagnetic energy is absorbed by the material. The real parts of permittivity and permeability (ε', μ') express the storage while the imaginary parts (ε'', μ'') express the dissipation.

Permittivity unit in SI (International System of Units) is Farads per meter $\left(\frac{F}{m}\right)$ and permeability unit is Henry per meter $\left(\frac{H}{m}\right)$.

In microwave electronics are often used the dimensionless quantities relative permittivity (ε_r) and relative permeability (μ_r)

$$\varepsilon_r = \frac{\varepsilon}{\varepsilon_o} = \frac{\varepsilon' - j\varepsilon''}{\varepsilon_o} = \varepsilon_r' - j\varepsilon_r'' \tag{2.3}$$

$$\mu_r = \frac{\mu}{\mu_o} = \frac{\mu' - j\mu''}{\mu_o} = \mu_r' - j\mu_r'' \tag{2.4}$$

where $\varepsilon_o = 8{,}854 \cdot 10^{12} \frac{F}{m}$ is the permittivity of the free space, $\mu_o = 4\pi \cdot 10^{-7} \frac{H}{m}$ is the permeability of free space, ε_r' is the relative dielectric constant and ε_r'' is the loss factor [Chen *et al.* 2004, pp. 8-9].

Another quantity that also used is the *electrical conductivity* (σ) which expresses a material's ability to conduct an electric current. It's unit in SI is Siemens per meter $\left(\frac{S}{m}\right)$. Related to permittivity is

$$\varepsilon'' = \frac{\sigma}{\omega} \tag{2.5}$$

and so

$$\varepsilon_r = \varepsilon_r' - j\frac{\sigma}{\varepsilon_o \omega} \tag{2.6}$$

2.2 Dielectric Materials

Permittivity and permeability are not constants but functions of frequency. The main mechanisms that contribute to the permittivity of a dielectric material are *conduction*, *dipolar relaxation*, *atomic polarization* and *electronic polarization*. In low frequencies ε'' is dominated by the influence of ion conductivity and in microwave frequencies the variation of permittivity is mainly caused by dipolar relaxation. In the infrared region and above the absorption peaks are mainly due to atomic and electronic polarizations.
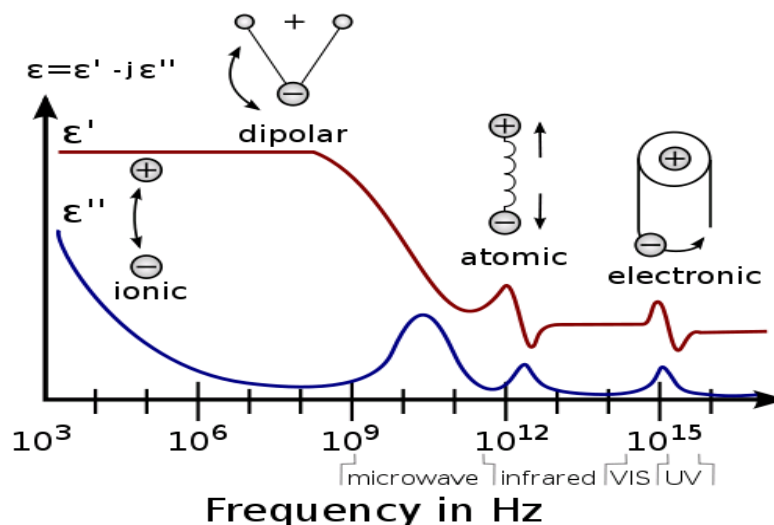
Figure 1. The permittivity of a hypothetical dielectric against frequency. Image used with the consent of Prof. Kenneth A. Mauritz, from the Wikimedia Commons (source page: http://www.usm.edu/polymer).

In Figure 1 the permittivity of a hypothetical dielectric against frequency is shown. At frequencies, up to $10\ GHz$, the permittivity of a dielectric material can be considered as constant against frequency. At microwaves it's decreasing and beyond $10\ THz$ there are some peaks and variance but in narrow range. More details on this diagram can be found in the literature [Ramo *et al.* 1994, Chen *et al.* 2004, p. 12].

Electronic polarization occurs in neutral atoms when an electric field displaces the surrounding electrons with respect to the nucleus. Atomic polarization occurs when adjacent positive and negative ions stretch under an applied electric field. Electronic and atomic

polarizations are of similar nature. If only these two polarizations are present the materials are almost lossless at microwave frequencies.

At microwave and millimeter-wave ranges the variations due to mainly dipolar relaxation and the Debye equations can be applied. The relative permittivity according to Debye theory is [Robert 1988, Chen *et al.* 2004, p. 13]

$$\varepsilon_r = \varepsilon_{r\infty} + \frac{\varepsilon_{r0} - \varepsilon_{r\infty}}{1 + j\beta} \tag{2.7}$$

with

$$\varepsilon_{r\infty} = \lim_{\omega \to \infty} \varepsilon_r \tag{2.8}$$

$$\varepsilon_{r0} = \lim_{\omega \to 0} \varepsilon_r \tag{2.9}$$

$$\beta = \omega\tau \tag{2.10}$$

where ω is the angular frequency $\omega = 2\pi f$, with f the frequency, and τ is the relaxation time. Permittivity due to Debye relaxation is determined by three parameters τ, $\varepsilon_{r\infty}$, ε_{r0}.

At sufficiently low frequencies there is no phase difference between the polarization and electric field and thus ε_{r0} is a real number. But the static permittivity ε_{r0} decreases as increasing temperature because of the increasing disorder and the relaxation time τ is inversely proportional to temperature as all the movements become faster at higher temperature. As at sufficiently high frequencies, as the period $\left(\frac{1}{f}\right)$ of electric field is much smaller than the relaxation time of the permanent dipoles, the orientations of the dipoles are not influenced by electric field and remain random and thus the permittivity at infinite frequency $\varepsilon_{r\infty}$ is a real number.

The relaxation phenomenon may be caused by different sources, in some cases, and the dielectric material has a relaxation-time spectrum. A moist material for example contains water molecules bound with different strength. The material exhibits a distribution of relaxation frequencies, depending on the moisture and the strength of binding water [Chen *et al.* 2004, pp. 13-14].

2.3 Microwave Methods

The *microwave methods* of measurements for materials characterization are divided in two types, *resonant* and *nonresonant*. Resonant methods give more accurate knowledge of dielectric properties over a limited frequency range or a single frequency, while the nonresonant methods give a general knowledge of electromagnetic properties over a frequency range. The resonant methods are the *resonator* method and the *resonator-perturbation method* [Chen *et al.*2004, pp. 40-42]. Nonresonant methods are the *reflection* methods and the *transmission/reflection methods* [Chen *et al.*2004, pp. 38-40]. This project is dedicated to two nonresonant methods.

2.4 Nonresonant Methods

In nonresonant methods from the impedance and the wave velocity in the material, the electromagnetic properties, *permittivity ε* and *permeability μ*, can be derived from the partial reflection of an incident wave from the interface between two materials.

In such a method a transmission line is needed to direct the wave to the material under test and then collect the reflected and/or the transmitted energy. This line can be coaxial, metallic waveguide, dielectric waveguide, planar transmission line and free space. In this project coaxial line and metallic rectangular waveguide has been used.

2.5 Microwave Network and Scattering Parameters

The concept of microwave network is to represent the responses of a microwave structure to external signals. The responses of a network to external circuits can be described by the input and output waves. A two-port network is presented in Figure 2.
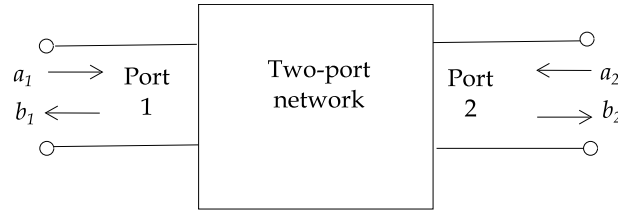
Figure 2. A two-port microwave network.

The input waves are a_i waves and b_i are the output waves. From port 1 we have input a_1 and output b_1 and from port 2 a_2 and b_2 respectively. Parameters a_i, b_i may be voltage or current.

The relations between the input $[a]$ and output waves $[b]$ are described by *scattering parameters* $[S]$, using matrices

$$[b] = [S][a] \tag{2.11}$$

or

$$\begin{bmatrix} b_1 \\ b_2 \end{bmatrix} = \begin{bmatrix} S_{11} & S_{12} \\ S_{21} & S_{22} \end{bmatrix} \begin{bmatrix} a_1 \\ a_2 \end{bmatrix} \tag{2.12}$$

where

$$[a] = \begin{bmatrix} a_1 \\ a_2 \end{bmatrix}, \ [b] = \begin{bmatrix} b_1 \\ b_2 \end{bmatrix} \text{ and } [S] = \begin{bmatrix} S_{11} & S_{12} \\ S_{21} & S_{22} \end{bmatrix} \tag{2.13}$$

If $a_i = 0$ ($i = 1 \ or \ 2$), the scattering parameters can be expressed as ratios (with $j = 1, 2$ and $i \neq j$)

$$S_{jj} = \frac{b_j}{a_j} \qquad\qquad (2.14)$$

$$S_{ij} = \frac{b_i}{a_j} \qquad\qquad (2.15)$$

Equation (2.14) shows that when port j is connected to a source and the other port is connected to a matching load, the reflection coefficient at port j is equal to S_{jj}

$$\varGamma_j = S_{jj} = \frac{b_j}{a_j} \qquad\qquad (2.16)$$

Equation (2.13) shows that when port j is connected to a source and port i is connected to a matching load, the transmission coefficient from port j to port i is equal to S_{ij}

$$T_{j\to i} = S_{ij} = \frac{b_i}{a_j} \qquad\qquad (2.17)$$

2.6 <u>Network Analyzers, Errors and Calibration</u>

To measure the four elements in a scattering matrix *network analyzers* are used. A network analyzer consists of a source, signal separation devices and detectors. Such a device can measure the four waves independently, two forward travelling waves a_1 and a_2, and two reverse travelling waves b_1 and b_2. By the combinations of these waves according to equations (2.14), (2.15) the scattering parameters can be obtained.

Measurements using network analyzers may have three kind of *errors*, *systematic*, *random* and *drift*. Random errors are unpredictable and they can be removed by making several measurements and taking the average values. Drift errors are caused by the change of working conditions and require a stable environment in terms of temperature, humidity etc to be suppressed. Systematic errors mainly include directivity, match, cross talk and frequency response. These errors are caused by imperfections in the measurement systems and most of them do not vary with time. They can be characterized through a *calibration* procedure and mathematically removed during the measurement process.

Calibration is a process which computes the systematic errors from measurements on known reference standards. When subsequent measurements are made the effects of the systematic errors are mathematically removed. There are two types of error corrections that can be done, response corrections and vector corrections. Response calibration is simple to perform but corrects only a few of the systematic error terms. Vector-error calibration can account for all major sources of systematic errors but requires more calibration standards and also requires that the network analyzer can measure both magnitude and phase data [Chen *et al.* 2004, pp. 119-123]. With further calibrations drift errors can be removed. In this Thesis the vector-error calibration has been used.

3. Reflection Methods

In a reflection method the sample of the material under test is connected to a certain position of a transmission line and so the impedance loading to the transmission line is changed. From the reflection because of this impedance discontinuity, electromagnetic properties can be derived, the *relative permittivity ε_r* and *the relative permeability μ_r* . There are two types of reflection methods corresponding to the type of reflection that is used, the *open-reflection method* for open-circuited reflection and the *shorted-reflection method* for short-circuited reflection. This project focuses on the open-reflection method.

The measurement fixture is called *probe*, or sensor, and is made from a transmission line. The measurement probes are specially designed to increase accuracy and sensitivity and to satisfy special requirements. In the most cases coaxial line is used, due to their broad frequency band, and so coaxial probes also [Chen *et al.* 2004, p. 142].

3.1 Open Circuited Reflection

In an open circuited reflection the material under test directly contacts the open end of the coaxial line. The impedances at the two sides of the interface are different and there is a reflection when electromagnetic wave incidents to the interface. The reflectivity is determined by the impedances of the media at the two sides of the interface. The impedance of the sample's side is related to the properties of the sample, and from the reflectivity at the interface, the properties of the sample can be obtained.

Both the permittivity and permeability can be obtained provided sufficient independent reflection measurements are made. However, in most cases only one independent measurement is made, so only one material property can be obtained. To obtain both permittivity and permeability, more complex experimental setups are needed [Chen *et al.* 2004, pp. 164-168].

As shown in Figure 3, the equivalent circuit of a reflection method consists of a transmission line of impedance Z_0, terminated to a load of impedance $Z(\varepsilon_r)$. The impedance $Z(\varepsilon_r)$ is a function of the relative permittivity ε_r of the sample. From the reflection measurement, $Z(\varepsilon_r)$ can be obtained and so ε_r can be derived from that.
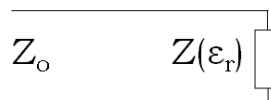

Figure 3. A transmission line of impedance Z_0 terminated to a load of impedance $Z(\varepsilon_r)$.

An objective function is defined as [Chen *et al.* 2004, p. 143]

$$F(\varepsilon_r) = Y_L(\varepsilon_r) - Y_m \qquad (3.1)$$

where $Y_L(\varepsilon_r)$ is the admittance calculated by using an aperture model and Y_m is the measured aperture admittance. The permittivity of the sample can be calculated by finding the zero of the function. There are four models of the of the open-ended coaxial probe for the calculation of $Y_L(\varepsilon_r)$.

3.2 Coaxial Line Reflection Method

Although all kind of transmission line can be used in the reflection method, mostly coaxial line is used and thus coaxial probes. This method is broadband, simple and convenient (non-destructive), has limited ε_r accuracy and is most accurate for liquids or semi-solids. The measurement fixture is called *coaxial dielectric probe*. The probe is usually into a flange, to provide suitable capacitance and ensure the repeatability of sample loading [Chen *et al.*2004 pp. 144-145, Li and Chen 1995, Stuchly and Stuchly 1980]. Such a probe is shown in Figure 4.
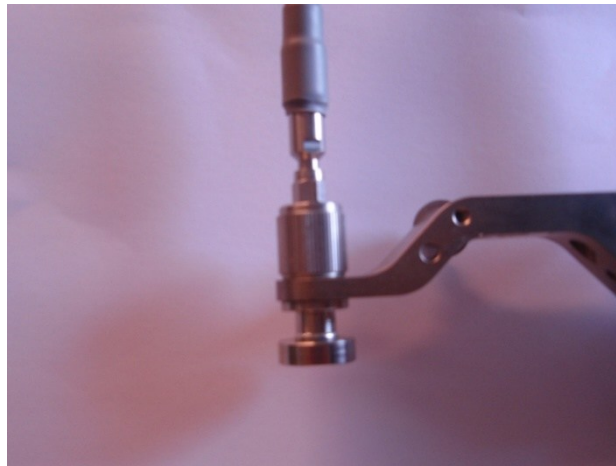

Figure 4. A coaxial probe with flange.

The open-ended coaxial probe is a cut off section of transmission line. The material is measured by immersing the probe into a liquid or touching it to the flat face of a solid (or powder) material. The fields at the probe end "fringe" into the sample and change as they come into contact with the material [Agilent 2006]. This method assumes the sample to be non-magnetic, isotropic and homogenous and to have a flat surface if it is a solid. Also the sample must be thick enough, "semi-infinite", much larger than the diameter of the aperture of the open-ended coaxial line, because this method assumes that interactions of the electromagnetic field with the non-contacting boundaries of the sample are not sensed by the probe. No air gaps must be between the probe and the sample.

The disadvantage of the coaxial line reflection method is the limited accuracy, under some conditions when compared to other methods like the transmission line method and resonator method.

3.3 Models of the Open-Ended Coaxial Probe

There are four typical models to describe the open-ended coaxial probes terminated by semi-infinite homogenous materials [Chen *et al.*2004 pp. 145-149, Pournaropoulos and Misra 1997, Bérubé *et al.*1996, Stuchly *et al.*1982, Athey *et al.*1982, Brady *et al.* 1981, Ghannouchi and Bosisio 1989, Stuchly *et al.*1994, Anderson *et al.*1994]

3.3.1 Capacitive model

The equivalent circuit of this model consists of two capacitances connected in parallel. The one, $C(\varepsilon_r)$, is related to the dielectric properties of the sample while the other, C_f, is the fringe field capacitance independent of these properties. When a dielectric sample with complex relative permittivity ε_r is connected to the probe, the equivalent capacitor will be changed and the reflection coefficient is given by

$$S_{11}^* = S_{11}e^{j\varphi} = \frac{1-j\omega Z_0[C(\varepsilon_r)+C_f]}{1+j\omega Z_0[C(\varepsilon_r)+C_f]} \qquad (3.2)$$

where $C(\varepsilon_r)=\varepsilon C_0$, C_0 is the capacitance of the air-filled parallel plate capacitor, ω is the measurement angular frequency ($\omega = 2\pi f$) and Z_0 is the characteristic impedance of coaxial line.

The complex relative permittivity is given by

$$\varepsilon_r = \frac{1-S_{11}^*}{j\omega Z_0 C_0(1+S_{11}^*)} - \frac{C_f}{C_0} \qquad (3.3)$$

Parameters C_f and C_0 must be obtained to calculate S_{11}^* and ε_r. Calibration of the open-ended probe with a standard sample with known dielectric permittivity can derive C_f and C_0. [Bérubé *et al.* 1996, Chen *et al.*2004 p. 146]

3.3.2 Radiation model or Antenna model

The coaxial probe is considered as a radiation source [Chen et al 2004 p. 146]. The equivalent circuit consists of two capacitors ($C_1, \varepsilon_r C_2$) and a conductance (G), all connected in parallel. The capacitance C_1 is independent of the material under test and is resulting from the fringe field inside the air-filled coaxial line. The capacitance $\varepsilon_r C_2$ expresses the presence of the material under test and is dependent on the permittivity of the test sample. The conductance G is the radiation conductance and is representing the power radiated from the end of the line [Pournaropoulos and Misra 1997, Stuchly and Stuchly 1980, Chen *et al.*2004 p. 146].

The normalized admittance is

$$\frac{Y}{Y_0} = j\omega C_1 Z_0 + j\omega\varepsilon_r C_2 + Z_0 G(\omega,\varepsilon_r) \qquad (3.4)$$

where Y_0 and Z_0 are the characteristic admittance and impedance of the line respectively, ε_r is the complex permittivity and ω the angular frequency.

For an infinitesimal antenna is [Burdette *et al.* 1980, Deschamps 1972]

$$G(\omega, \varepsilon_r) = \varepsilon_r^{5/2} G(\omega, \varepsilon_0) \tag{3.5}$$

and so is

$$\frac{Y}{Y_0} = j\omega C_1 Z_0 + j\omega \varepsilon_r C_2 + \varepsilon_r^{5/2} G(\omega, \varepsilon_0) \tag{3.6}$$

The admittance can be expressed as

$$\frac{Y}{Y_0} = K_1 + K_2 \varepsilon_r + K_3 \varepsilon_r^{5/2} \tag{3.7}$$

The factors K_1, K_2, K_3 are complex and they can be determined by using three known media in the calibration procedure. The complex admittance refers to the plane of the end of the coaxial geometry.

A more accurate model is [Gajda and Stuchly 1983,]

$$\frac{Y}{Y_0} = K_1 + K_2 \varepsilon_r + K_3 \varepsilon_r^2 + K_4 \varepsilon_r^{5/2} \tag{3.8}$$

where the frequency dependence of C_1 has been considered.

Another approximation is [Staebell and Misra 1990,]

$$\frac{Y}{Y_0} = K_1 \varepsilon_r + K_2 \varepsilon_r^2 + K_3 \varepsilon_r^{5/2} \tag{3.9}$$

using quasi-static analysis.

An approximation for very low frequency is [Staebell and Misra 1990,]

$$\frac{Y}{Y_0} = K_1 \varepsilon_r + K_2 \varepsilon_r^2 \tag{3.10}$$

For all models, determination of parameters K_i is achieved with calibration.

The model (3.10) is the model used in this project.

3.3.3 Virtual line model

In an open-ended method using a coaxial probe, the material under test where the probe is terminated, can be modeled as a virtual part of transmission line. The transmission line consists of a part of physical line with length D and a part of visual line with length L, which models the material under test [Ghannouchi and Bosisio 1989, Chen *et al.*2004 pp147-148].

The complex permittivity of the material under test related to the measured S_{11m} is

$$\varepsilon_d = \frac{-jc\sqrt{\varepsilon_t}}{2\pi f L} \frac{1 - S_{11m}e^{2j\beta_t D}}{1 + S_{11m}e^{2j\beta_t D}} \cot\left(\frac{2\pi f L\sqrt{\varepsilon_d}}{c}\right) \tag{3.11}$$

where f is the measurement frequency and c is the speed of light, S_{11m} is the complex reflection coefficient measured at the reference plane before the physical line (at the analyzer port), β_t is the propagation constant in the coaxial probe and ε_t is the permittivity of the material inside the physical coaxial line.

The values D and L can be derived by calibration using two well-known dielectric materials like air and deionized water.

3.3.4 Rational function model

In this model, the coaxial probe is immersed in the material under test. The energy storage in the near-field region, the evanescent mode of the guide and the radiation effects have to be considered [Chen *et al.* 2004 pp148-149, Stuchly *et al.* 1994, Anderson *et al.* 1994].

The admittance of the probe is

$$\frac{Y}{Y_0} = \frac{\sum_{n=1}^{4}\sum_{p=1}^{8} a_{np}(\sqrt{\varepsilon_r})^p (j\omega a)^n}{1 + \sum_{m=1}^{4}\sum_{q=1}^{8} \beta_{mq}(\sqrt{\varepsilon_r})^q (j\omega a)^m} \tag{3.12}$$

where Y is the admittance at the end of the coaxial probe, Y_0 is the characteristic admittance of the coaxial probe, ε_r is the complex relative permittivity of the sample, a is the inner diameter of the line and a_{np} and β_{mq} are the coefficients of the model.

To derive the complex permittivity of the sample from the measured complex admittance values referred at the end of the probe we solve the inverse problem [Anderson *et al.* 1994]

$$\sum_{i=0}^{8}(b_i - Y c_i)\left(\sqrt{\varepsilon_r}\right)^i = 0 \tag{3.13}$$

with
$$b_p = \sum_{m=1}^{4} a_{mp}(j\omega a)^m \quad (p = 1,2\ldots8) \tag{3.14}$$

$$b_0 = 0 \tag{3.15}$$

$$c_q = \sum_{m=1}^{8} \beta_{mq}(j\omega a)^m \quad (q = 1,2\ldots8) \tag{3.16}$$

$$c_0 = 1 + \sum_{m=1}^{8} \beta_{m0}(j\omega a)^m \tag{3.17}$$

No calibration parameters are needed, and the model parameters a_{np} and β_{mq} have been established and optimized [Bérubé *et al.*1996].

The virtual line model gives the best results for permittivity measurements, while the results obtained with the antenna model are also accurate except at low frequencies [Bérubé *et al.*1996]. The high accuracy of the antenna model (3.10) in combination with the easy implementation of the calibration procedure in [Staebell and Misra 1990] were the reasons for the choice of this model.

3.4 Calibration for the Coaxial Probe

The quasi-static formula (3.9) that was given above, can be approximately expressed like [Staebell and Misra 1990]

$$Y_L = j \frac{2\omega I_1}{[\ln(b/a)]^2} \varepsilon - j \frac{\omega^3 \mu_0 I_2}{[\ln(b/a)]^2} \varepsilon^2 + \frac{\pi \omega^4 \mu_0^{3/2}}{12} \left[\frac{b^2 - a^2}{\ln(b/a)} \right]^2 \varepsilon^{5/2} \qquad (3.18)$$

where ω is the angular frequency, μ_0 is the permeability of the free space, ε_r is the relative permittivity of the material, a is the inner and b the outer radius of the coaxial aperture respectively and I_1, I_2 are triple integrals dependent only on the radii [Misra 1987].

The first term of the equation (3.18) represents a capacitance, the second a frequency-dependent capacitance and the third a radiation conductance.

An equivalent two port network (error box) between the meter (analyzer) and the coaxial opening is being considered. The admittance of the aperture terminated by a sample is evaluated from the measured reflection coefficient after calibrating the system. The calibration is done using three standard materials [Staebell and Misra 1990, Marsland and Evans 1987, Chabbra *et al.* 1989]

$$\frac{Y_s - Y_1}{Y_s - Y_2} \cdot \frac{Y_3 - Y_2}{Y_1 - Y_3} = \frac{\delta_{s1} \delta_{32}}{\delta_{s2} \delta_{13}} \qquad (3.19)$$

where Y_1, Y_2, Y_3, are aperture admittances with standards respectively, Y_s is the desired aperture admittance terminated by the sample material and

$$\delta_{ij} = \Gamma_i - \Gamma_j \qquad (3.20)$$

with Γ_n representing the measured reflection coefficient for the nth material.

From the measured data (Γ_n) the right-hand side of (3.19) is determined. The admittances Y_1, Y_2, Y_3 are calculated from (3.18) for known values of ε for the three standards.

To avoid calculating the radii a and b, and the integrals I_1 and I_2 a fourth standard is used.

The equation (3.18) can be written as

$$y_L = \varepsilon_r + \xi \varepsilon_r^2 + \xi_1 \varepsilon_r^{2.5} \qquad (3.21)$$

which is equivalent to the (3.9) and where ξ and ξ_1 are constants dependent on the frequency and the dimension of the aperture, and y_L is a normalized parameter of aperture admittance Y_L.

At low microwave frequencies the radiation from the coaxial aperture can be neglected, so the equation (3.21) can approximately be written as

$$y_L \cong \varepsilon_r + \xi \varepsilon_r^2 \tag{3.22}$$

which is equivalent to (3.10).

The aperture parameter y_s can be determined from equations (3.19) and (3.22). If the third standard is short calibration circuit the parameter y_s can be used to calculate the complex permittivity ε_r

$$y_s = \frac{(y_1 + \Delta' y_2)}{(1 + \Delta')} \tag{3.23}$$

where

$$\Delta' = \frac{\delta_{s1} \delta_{32}}{\delta_{s2} \delta_{13}} \tag{3.24}$$

From the equation (3.22) the values y_1 and y_2 are calculated for known relative permittivities of the standards 1 and 2 respectively at the operating frequency.

From the measured reflection coefficients (Γ_n) and known complex permittivities for standards 1, 2 and 4, the constant ξ of (3.22) is calculated

$$\xi = \frac{(1 + \Delta)\,\varepsilon_{r4} - \varepsilon_{r1} - \Delta\varepsilon_{r2}}{\varepsilon_{r1}^2 + \Delta\varepsilon_{r2}^2 - (1 + \Delta)\varepsilon_{r4}^2} \tag{3.25}$$

and

$$\Delta = \frac{\delta_{41} \delta_{32}}{\delta_{42} \delta_{13}} \tag{3.26}$$

The relative complex permittivity ε_r is then calculated from (3.22). That is a second order equation which gives two roots. The selection of the root is made by the sign of the imaginary part. This has to be negative in order to express the loss and so the root with the negative imaginary part is chosen.

4. Transmission/Reflection methods

The transmission/reflection methods consist a category of nonresonant methods. In this kind of method, the sample under test is placed in a segment of transmission line, usually a waveguide or a coaxial line. The electromagnetic properties of the material under test, its permittivity and permeability, can be derived from the scattering parameters. In such a method all the four scattering parameters can be measured. The complex permittivity and permeability, the sample length and the positions of the two reference planes are the main variables contained in the relevant scattering equations of a transmission/reflection measurement. Although for a coaxial line the cutoff wavelength is infinity, the more difficult placement of a sample in such a line leads to more often use of waveguides and especially rectangular ones.

4.1 Basic Principle

A segment of a rectangular waveguide where a sample has been placed, filling the line and leaving no air gaps is a typical measurement configuration.
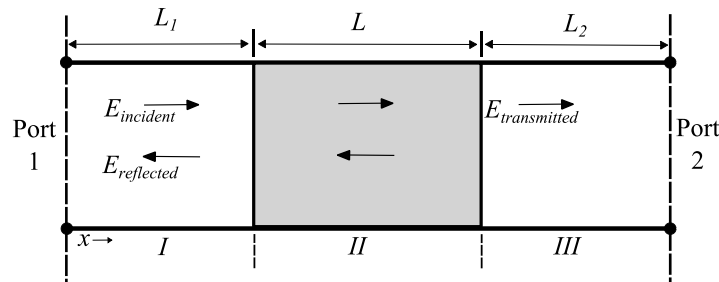
Figure 5. Incident, transmitted and reflected electromagnetic waves in a filled transmission line.

In Figure 5 is shown such a segment whose axis is in x-direction same with the propagation direction. The electric fields at the three sections of the transmission line are E_I, E_{II} and E_{III}. For a normalized incident wave is [Baker -Jarvis 1990, Chen *et al.* 2004 pp. 175-176]

$$E_I = e^{(-\gamma_o x)} + C_1 e^{\gamma_o x} \tag{4.1}$$

$$E_{II} = C_2 e^{(-\gamma x)} + C_3 e^{\gamma x} \tag{4.2}$$

$$E_{III} = C_4 e^{(-\gamma_o x)} \tag{4.3}$$

with

$$\gamma_o = j\sqrt{\left(\frac{\omega}{c}\right)^2 - \left(\frac{2\pi}{\lambda_c}\right)^2} \tag{4.4}$$

$$\gamma = j\sqrt{\left(\frac{\omega\mu_r\varepsilon_r}{c}\right)^2 - \left(\frac{2\pi}{\lambda_c}\right)^2} \tag{4.5}$$

the propagating constants in the line filled with air and the sample respectively, where μ_r is the complex permeability, ε_r is the complex permittivity c is the speed of light in vacuum, ω is the angular frequency and λ_c is the cutoff wavelength, with $\lambda_c = 2a$ where a is the width of the waveguide. The constants C_i $(i = 1,2,3,4)$ can be determined from the boundary conditions on the electric and the magnetic field [Chen *et al.* 2004 p. 176]

The total length of the transmission line can be expressed as

$$L_{air} = L_1 + L + L_2 \tag{4.6}$$

where L is the length of the sample and L_1 and L_2 are the distances from the respective ports to the sample faces corresponding to the three sections defined.

The scattering parameters of this two-port line can be obtained, and as the scattering matrix is symmetric ($S_{12} = S_{21}$), we have [Baker-Jarvis 1990, Chen *et al.* 2004 p 176]

$$S_{11} = R_1^2 \frac{\Gamma(1-T^2)}{1-\Gamma^2 T^2} \tag{4.7}$$

$$S_{22} = R_2^2 \frac{\Gamma(1-T^2)}{1-\Gamma^2 T^2} \tag{4.8}$$

$$S_{21} = R_1 R_2 \frac{\Gamma(1-T^2)}{1-\Gamma^2 T^2} \tag{4.9}$$

where R_1 and R_2 are the reference plane transformations at two ports:

$$R_i = e^{(-\gamma_o L_i)} \quad (i = 1,2) \tag{4.10}$$

The reflection coefficient is

$$\Gamma = \frac{(\gamma_0/\mu_0) - (\gamma/\mu)}{(\gamma_0/\mu_0) + (\gamma/\mu)} \tag{4.11}$$

and the transmission coefficient is

$$T = e^{(-\gamma L)} \tag{4.12}$$

For the empty sample holder we have

$$S_{21}^0 = R_1 R_2 e^{(-\gamma_o L)} \tag{4.13}$$

The unknown quantities are usually seven ε_r', ε_r'', μ_r', μ_r'', R_1, R_2, L and we have nine equations (4.6 - 4.13). The overdetermined system of equations can be solved in many ways. Usually the length L of the sample is known. L_1, L_2 are also often known, and thereby R_1 and R_2. If the material is nonmagnetic $\mu_r = 1$, so $\mu_r' = 1$ and $\mu_r'' = 0$.

4.2 Nicolson-Ross-Weir algorithm

The Nicolson-Ross-Weir (NRW) algorithm [Nicolson-Ross 1970, Weir 1974, Chen *et al.* 2004 pp. 177-178] combines the equations (4.7), (4.8) and derives formulas for the calculation of permittivity and permeability.

The reflection coefficient is

$$\Gamma = X \pm \sqrt{X^2 - 1} \qquad (4.14)$$

with

$$X = \frac{(S_{11}^2 - S_{21}^2) + 1}{2 S_{11}} \qquad (4.15)$$

and the appropriate sign is chosen so that $|\Gamma| \leq 1$ in order to express the passivity of the sample.

The transmission coefficient is

$$T = \frac{(S_{11} + S_{21}) - \Gamma}{1 - (S_{11} + S_{21})\Gamma} \qquad (4.16)$$

The complex permeability is calculated from

$$\mu_r = \frac{1 + \Gamma}{(1 - \Gamma)\Lambda \sqrt{(1/\lambda_0^2) - (1/\lambda_c^2)}} \qquad (4.17)$$

and the complex permittivity from

$$\varepsilon_r \mu_r = \lambda_0^2 \left(\frac{1}{\Lambda^2} + \frac{1}{\lambda_c^2} \right) \qquad (4.18)$$

with

$$\frac{1}{\Lambda^2} = -\left[\frac{1}{2\pi D} \ln \left(\frac{1}{T} \right) \right]^2 \qquad (4.19)$$

where λ_c is the cutoff wavelength of the transmission line section, λ_0 the free space wavelength and $Re \left(\frac{1}{\Lambda} \right) = \frac{1}{\lambda_g}$ where λ_g is the transmission line guide wavelength.

The equation (4.19) has an infinite number of roots since the imaginary part of the logarithm of a complex quantity (T) is equal to the angle of the complex value plus $2\pi n$, where n is equal to the integer of (L/λ_g). This equation is ambiguous because the phase of the transmission coefficient T does not change when the length of the material is increased by a multiple of wavelength.

The unwrapping method [Chen *et al.* 2004 pp. 177-178], can be used to solve the problem of phase ambiguity. Determination of the initial phase is needed and then phase unwrapping. For a sample with constant permittivity over a wide frequency range, the phase of T fluctuates

between $\pm\pi$. Phase ambiguity arises from the phase wrapping effect. Equivalent to phase unwrapping is to obtain the correct additive constant of $2\pi n$.

A simple and common way to unwrap the phase is by detecting a jump in phase value of more than π from one measurement frequency to the next and then shifting all the subsequent phases by 2π in the opposite direction.

Another important observation on permittivity and permeability are spurious peaks when the sample is a multiple of half wavelength of the microwave within the sample. In terms of small reflection data this can be explained. For low loss, multiple of half-wavelength slabs the reflection is ideally zero and so only transmission data are available for the computation of ε_r and μ_r. If is known that $\mu_r = 1$, ε_r can be calculated accurately from Equation (4.18).

4.3 Transformation of Reference Planes

In the case of a rectangular waveguide filled with a sample, the reference planes of the scattering parameters have to be transformed. The waveguide consists of two parts connected with a sample holder between them. The sample is placed in the sample holder, which has edges at planes 3 and 5 as it shown in Figure 6.
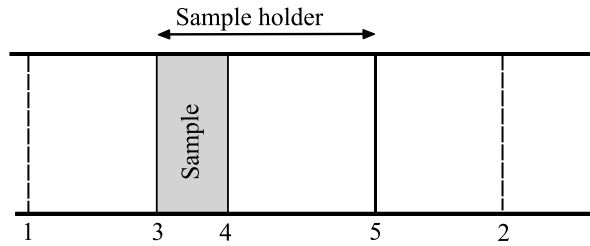
Figure 6. A filled waveguide. The reference planes 1, 2 are transferred to sample's edges 3, 4.

The calibration planes 1, 2 are defined by a calibration procedure inside the network analyzer to which the waveguide is connected. These planes have to be transferred to the sample's edges which are the planes 3 and 4. This transformation is very important especially when the phase of the scattering parameters is studied. This procedure has been illustrated [Larsson, Sjöberg and Elmkvist 2011] as a function of temperature.

4.4 Correction for Air Gaps

In the case of an air gap existence between the sample and the waveguide, the measured electromagnetic properties (the output of the NRW algorithm) are [Larsson, Sjöberg and Elmkvist 2011]

$$\varepsilon_m = \left(\frac{1-\Delta}{\varepsilon_s} + \frac{\Delta}{\varepsilon_g}\right)^{-1} \tag{4.20}$$

$$\mu_m = (1-\Delta)\mu_s + \Delta\mu_g \tag{4.21}$$

where ε_s and μ_s are the sample properties, ε_g and μ_g are the gap properties and the volume fraction of the air gap is $\Delta = (b - b_s)/b$. The sample and waveguide heights b_s and b respectively are shown in Figure 7.
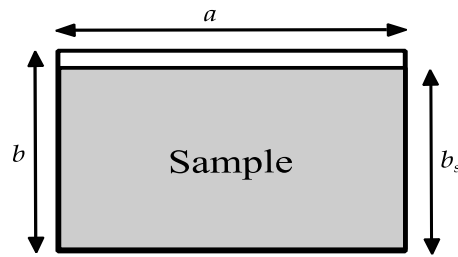

Figure 7. A sample partially filling a rectangular waveguide leaving a small air gap.

5. Experiments and Results

5.1 <u>Experiments with a Coaxial Probe</u>

In this part of the Thesis the experiments where a coaxial probe used are presenting

5.1.1 **The Measurement Procedure**

The experimental setup that was used is shown below. It consists of the coaxial probe, an HP 8720C Network Analyzer, a personal computer equipped with the control software and a coaxial cable. The coaxial probe is attached to a stable arm in order to remain motionless throughout the experiment. The coaxial probe is an Agilent 85070E high temperature probe, with frequency range 200 MHz – 20 GHz. The software that was used is the "Labview: Virtual Array System Control Software". The frequency range of the measurements was 50 MHz – 20 GHz with 401 points. The IF Bandwidth of the analyzer was settled 30 Hz and the output power was 10 mV.

The experiment took place in the Chemistry Lab of Electrical and Information Technology (EIT) department of Faculty of Engineering (Lunds Tekniska Högskola - LTH) of Lund University.

The measured elements were the air (open standard), the short standard, deionized water, pure ethanol (99%), isopropyl alcohol and saline (0.9% g/l). Each element was measured three times. The calibration standards were water (Γ_1), air (open) (Γ_2), short (Γ_3) and ethanol (Γ_4).

For known permittivities of water and ethanol, the Debye model as described in [Kaatze 1989, Debye 1929] was used. The complex permittivity as a function of frequency f is

$$\varepsilon(f) = \varepsilon(\infty) + \frac{\varepsilon(0) - \varepsilon(\infty)}{1 + j\omega\tau} \qquad (5.1)$$

where $\varepsilon(0)$ is the low frequency permittivity, $\varepsilon(\infty)$ is the extrapolated high-frequency permittivity, τ is the relaxation time and ω is the angular frequency.

For room temperature (25 $^{\mathrm{o}}$C) for the water is [Kaatze 1989]

$$\varepsilon(0) = 78.36, \qquad \varepsilon(\infty) = 5.2, \qquad \tau = 8.27 \text{ ps}$$

and it is shown in the Figure 8
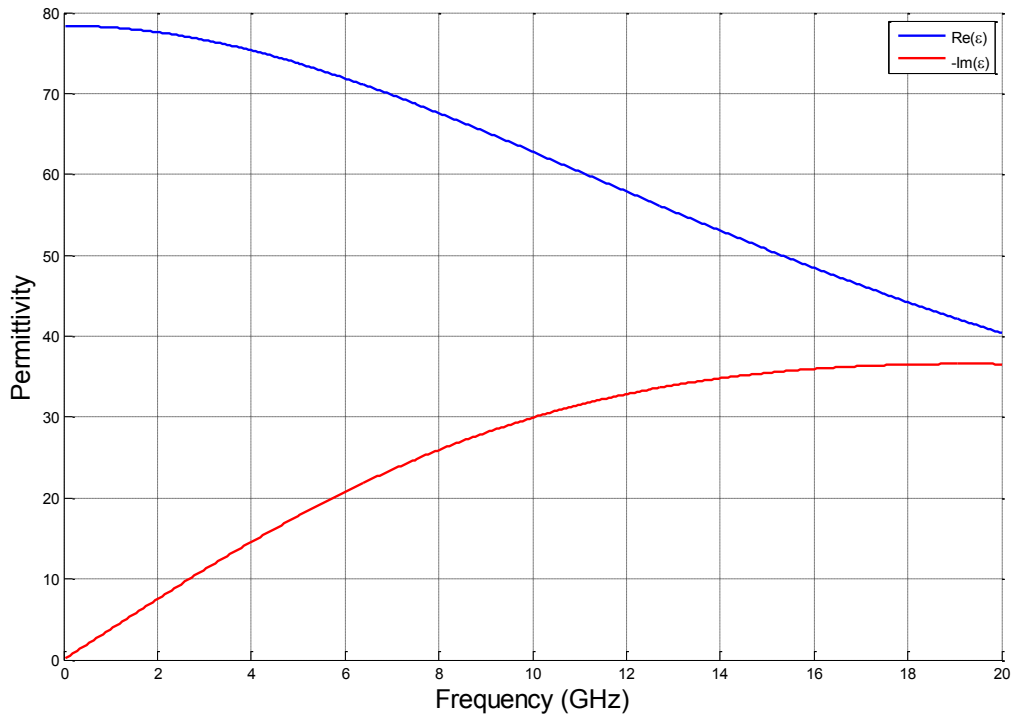
Figure 8. Permittivity of water according to the Debye model.

One can observe that the real part of permittivity of water is decreasing while the negative imaginary part is increasing against frequency. Both the decrease of the real part and the increase of the negative imaginary part are not sharp against frequency and this is due to the relatively small relaxation time. The real part begins at 78.36 and becomes 40.37 at 20 GHz. The negative imaginary has values from 0.19 until 36.56. This behavior due to the dipolar relaxation at microwave and millimeter-wave ranges.

For the ethanol is [Grant *et al.* 1989, Frellner-Feldegg 1969, Suggett *et al.* 1970] for room temperature

$$\varepsilon(0) = 24.4, \qquad\qquad \varepsilon(\infty) = 4.8, \qquad\qquad \tau = 140 \text{ ps}$$

The permittivity of ethanol is presented in Figure 9. The real part has values from 24.36 until 4.86 and the negative imaginary has range from 0.86 to 1.11. The relaxation time for ethanol is 17 times bigger than the water's and so the reduce of the real part is sharp. After 8 GHz it is approximately 5. The negative part is increasing from 0-1.15 GHz where has its maximum value 9.8 and then decreases till 1.11. These data are used for the calibration.

For the calibration the air permittivity is assumed $\varepsilon_r = 1$.
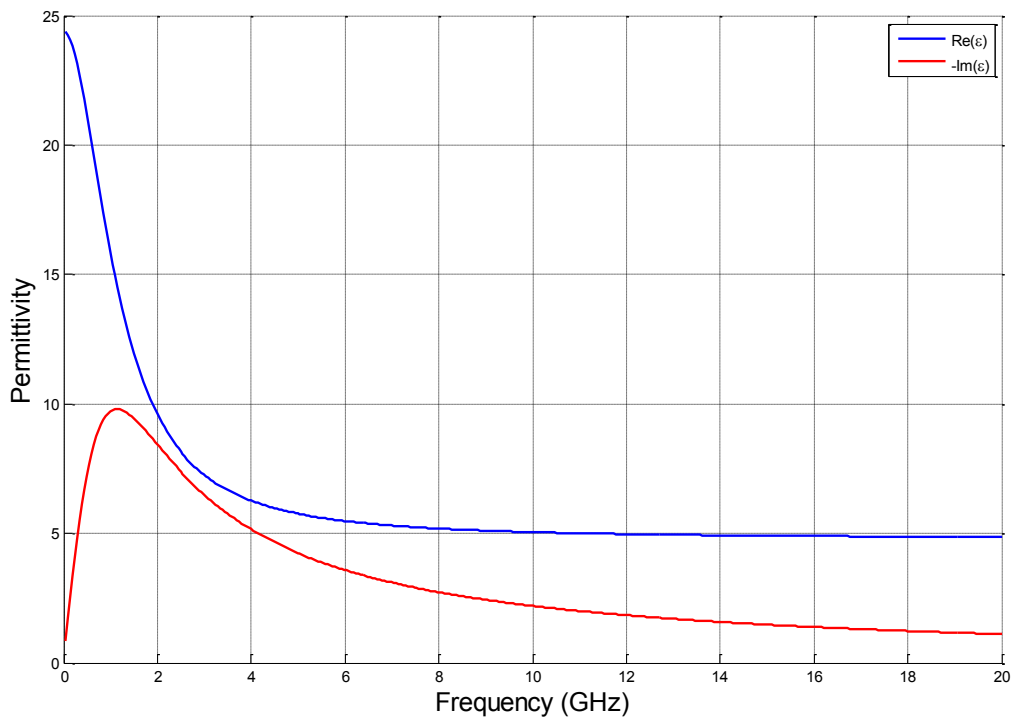
Figure 9. Permittivity of ethanol.

In the photos in Figures 10 and 11 the whole experimental setup is shown, the arm where the probe was stabilized, the network analyzer, the short standard, the short standard on the probe, and a liquid under measurement.

a.
b.

Figure 10. The experimental setup for the coaxial reflection measurements, a. The whole setup consists of the network analyzer, a computer, the coaxial probe with the short standard on it, b. The short standard.
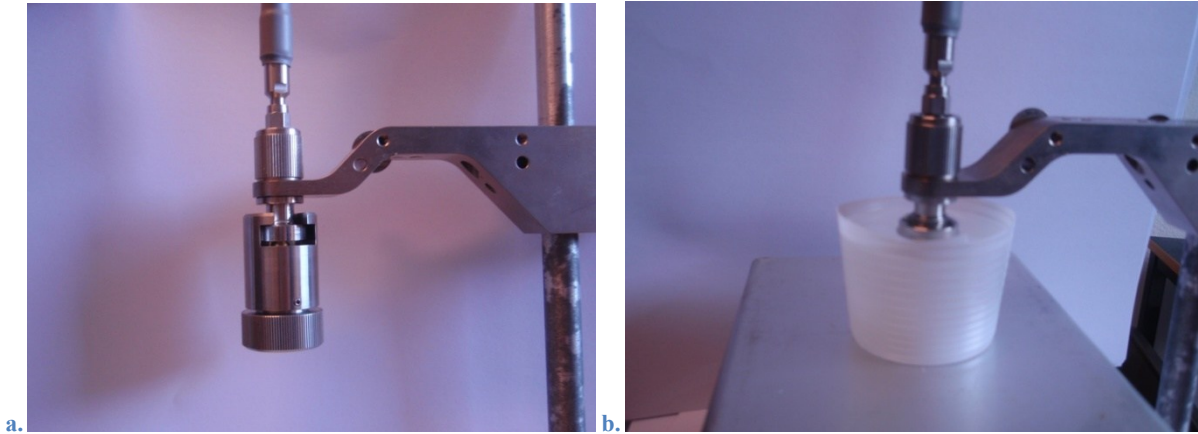
Figure 11. a. The short standard on the probe and b. The coaxial probe in a liquid sample.

5.1.2 Results of the Reflection Experiments

In Figure 12 the permittivity of saline as it measured is shown. The behavior of saline in frequencies lower than 2 GHz is due to its ionic conductivity. At the imaginary part of Equation (2.6) when the frequency is very small –tends to zero- this term is dominated by conductivity term σ/ω which takes extremely high values –tends to infinity.

From 2 GHz and above the permittivity of saline is similar to water's. The real part has values from 75.4 to 40 and the imaginary from 21.1 up to 36.8.
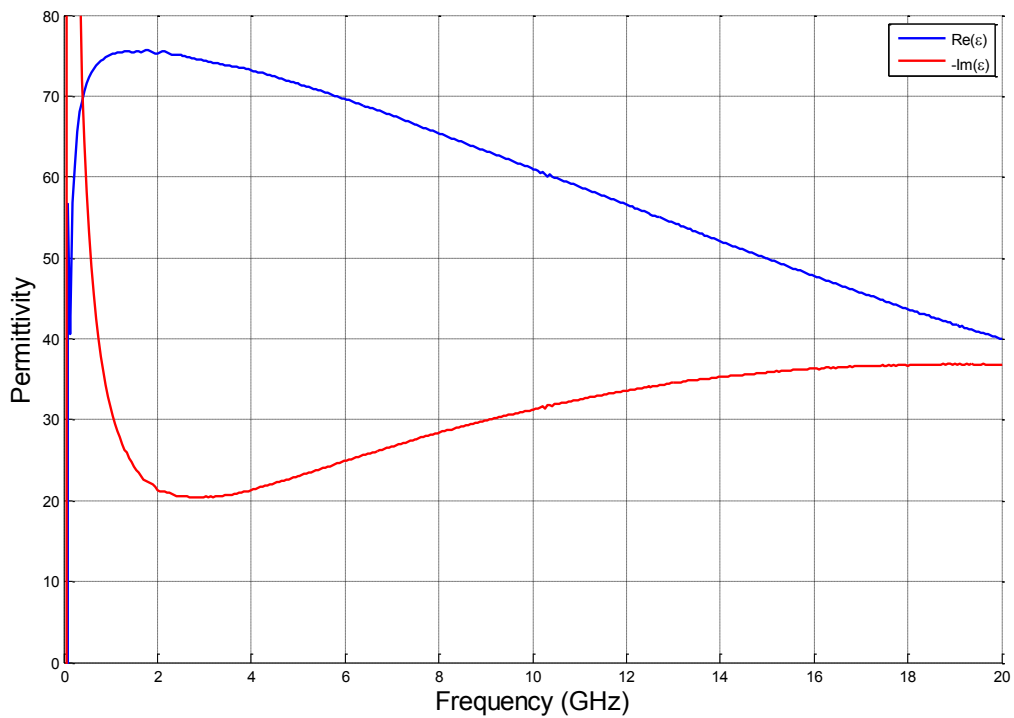
Figure 12. The permittivity of saline 0.9 up to 80.
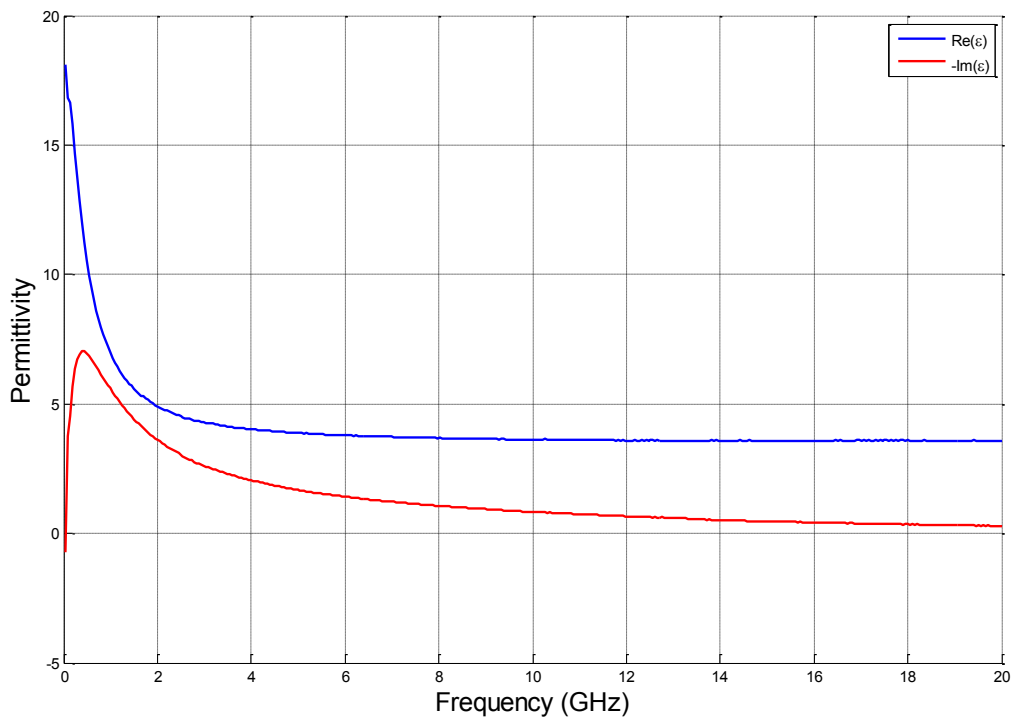
Figure 13. The permittivity of isopropyl alcohol.

In Figure 13 the permittivity of isopropyl alcohol as it measured is shown. It is similar to that of ethanol which is expected since they are both alcohols and have similar chemical composition. The real part has maximum value 18.1 and minimum 3.58. From 5 GHz and above is approximately 3.6. Similarly the negative imaginary part of isopropyl alcohol has range from -0.74 to 0.3 with maximum value 7.06 at 0.4 GHz. The relaxation time of isopropyl alcohol can be calculated from the maximum of the imaginary part and by using the Equations (2.7) and (2.10) at 400 ps, higher than ethanol's.

To have a view on the noise, a plot of air's permittivity is given in Figure 14 although this material has been used as a calibration standard. Two different measurements have been used, one for the calibration and one for permittivity calculation.
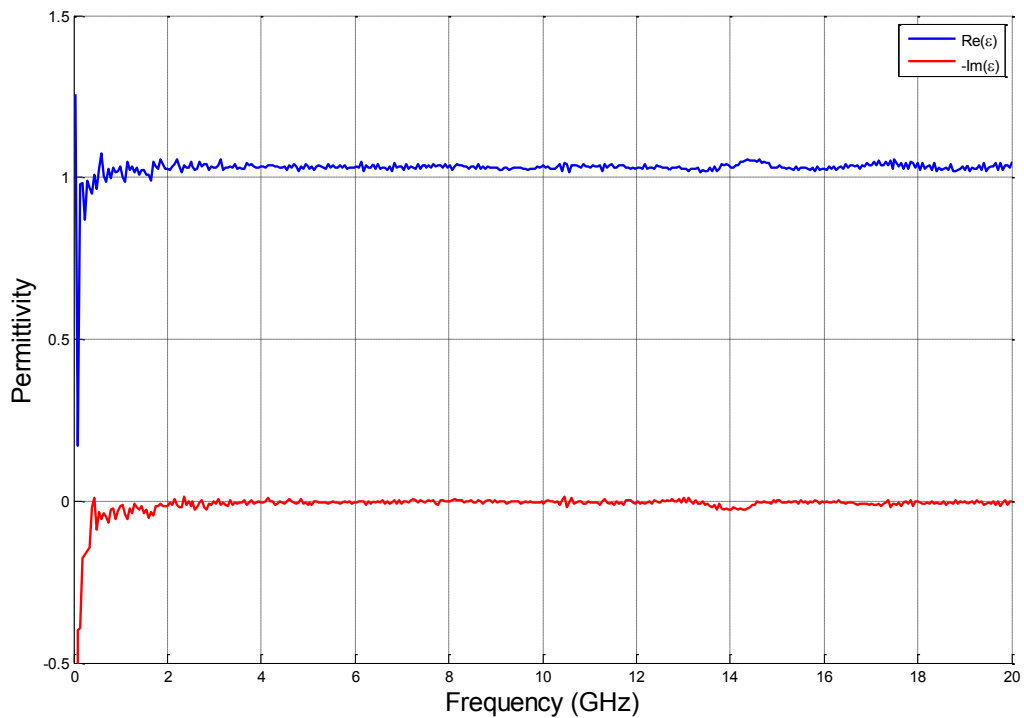
The real part of air's permittivity is above 1 and this is reasonable since lower value than 1 would correspond to a speed of light greater than that in vacuum.

Afterwards, measurements using a plastic foil around the coaxial probe were made. The plastic foil is used to protect the probe when measuring solid surfaces which can scratch and damage the probe.

Below are presented some measurements on solid samples of materials like (Expanded Polystyrene) EPS, Rohacell, and wood. EPS and Rohacell are soft materials and the touch with the probe can be considered good enough. The permittivity of these two materials is similar to permittivity of air.
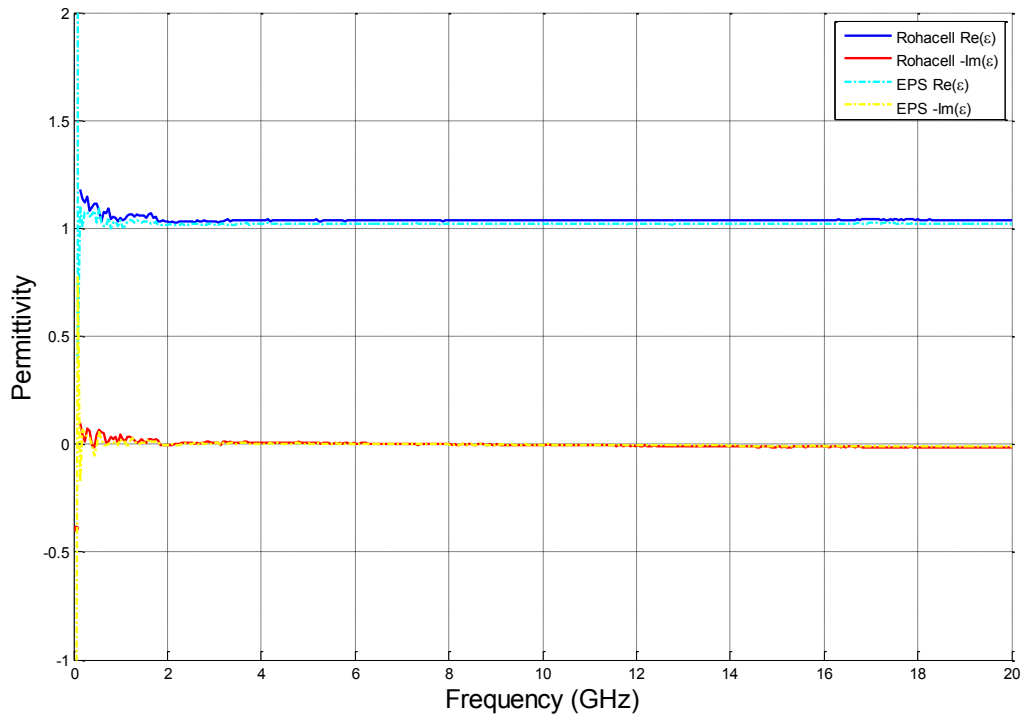
Figure 15. The permittivity of Rohacell and EPS.

In Figure 16 the permittivity of the wood sample is shown. For the hard wood the connection with the probe cannot be considered very good. A very little increase in real part and a decrease in the negative imagine exist. The real part is approximately 1.25.
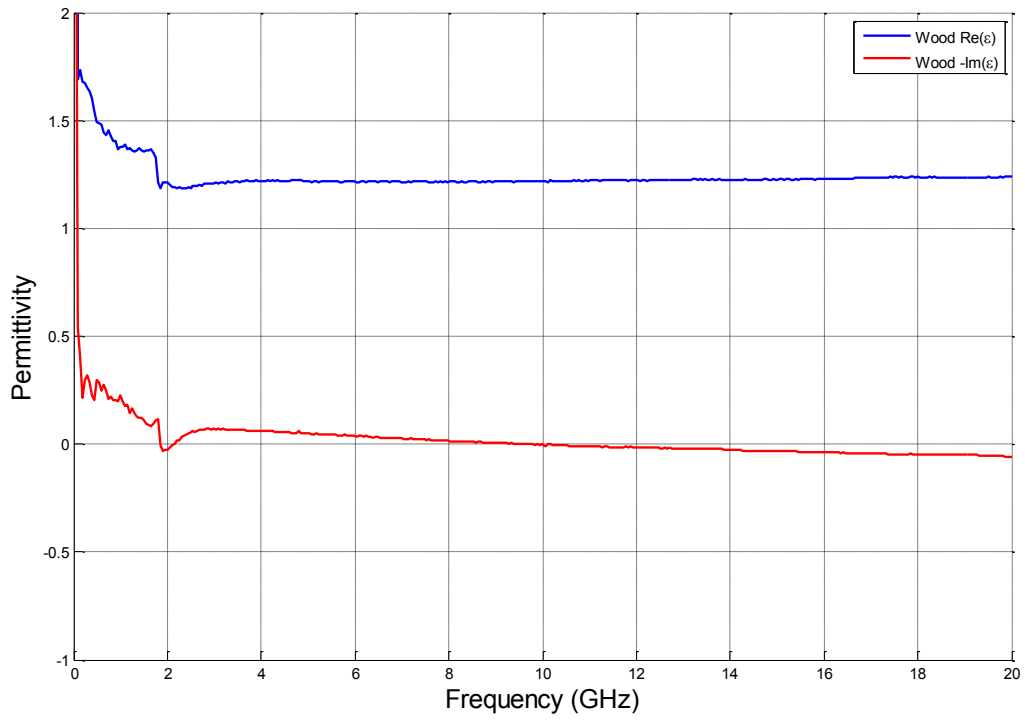
Figure 16. Permittivity of a wooden sample.

Some measurements on the EPS and rubber samples took place without the plastic foil since these materials are not dangerous for the probe (Figures 17 and 18).
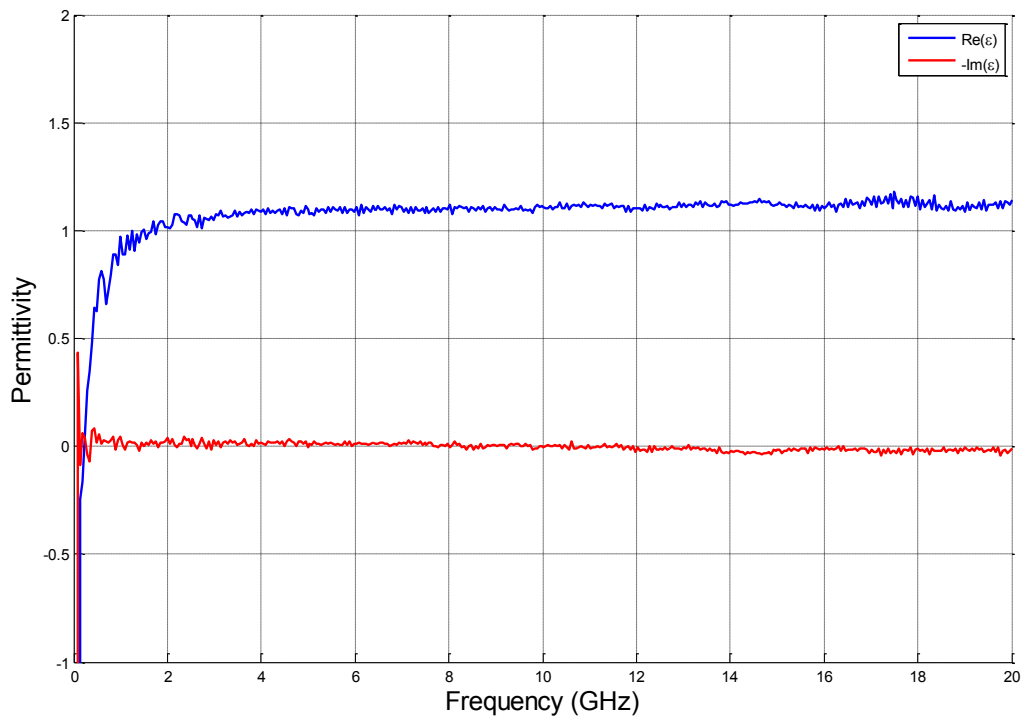
Figure 17. Permittivity of EPS measured without using the plastic foil on the probe.
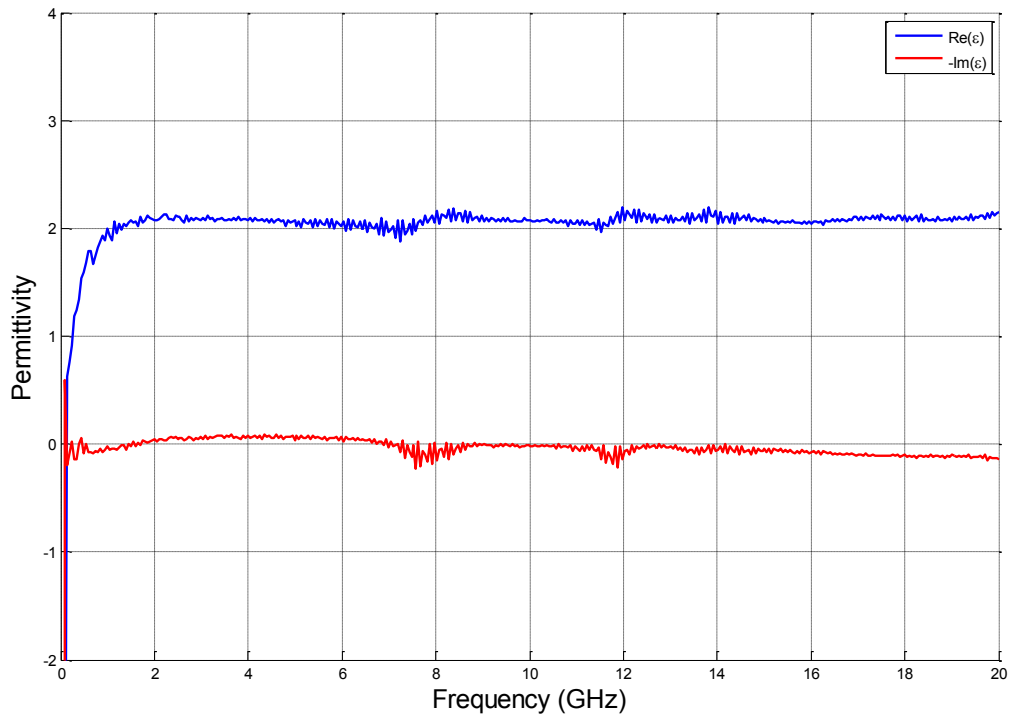
Figure 18. The permittivity of a rubber sample.

For the EPS some differences with the other measurement can be observed due to the presence of air between the sample and the probe. In the rubber measurement there are many abnormalities due to the not good touch of the surface with the probe. Its permittivity constant is approximately 2.1.

Below are given two diagrams to show the problem of choice between the two roots of Equation (3.22). The measured water's permittivity using the plastic foil on the probe together with its theoretical value is given. In Figure 19 the first root is presented and in Figure 20 the second.
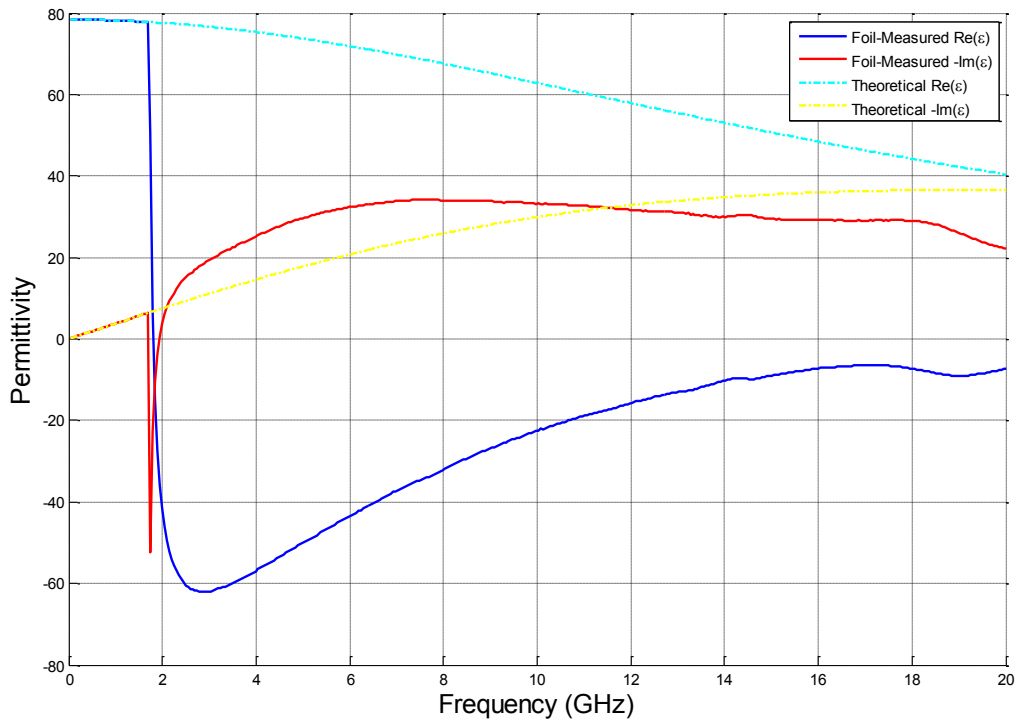
Figure 19. The first root of Equation (3.22) for measurement of water using the plastic foil on the probe.
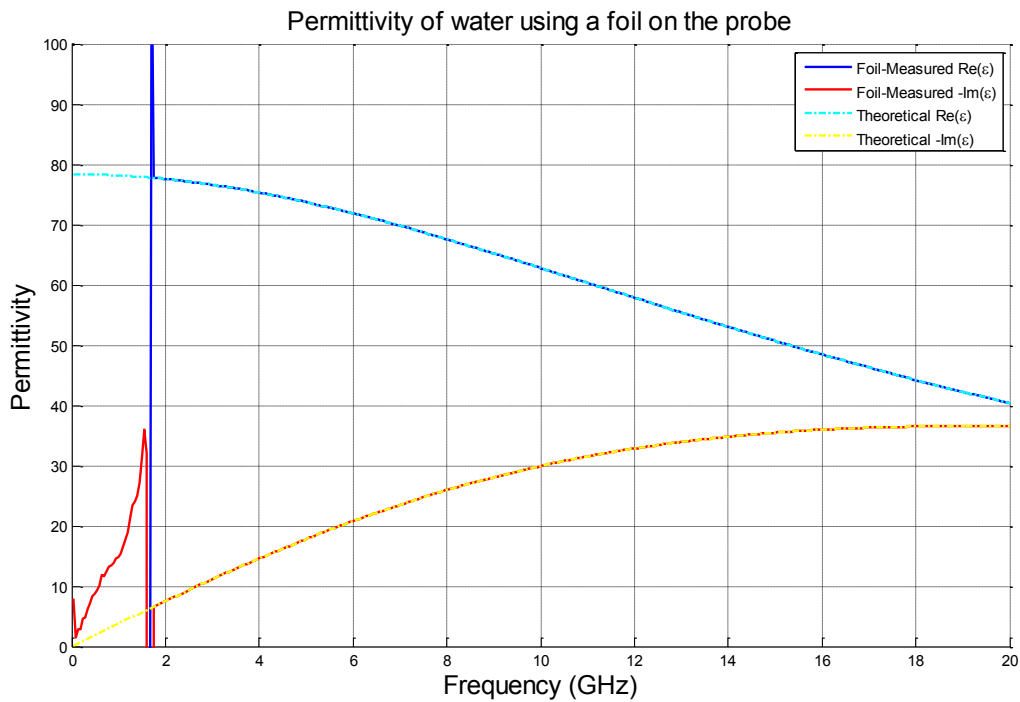
Figure 20. The second root of Equation (3.22) for measurement of water using the plastic foil on the probe.

At 1.7 GHz is the change frequency. Below 1.7 GHz the first root is correct and above that point the second root.

In the next Figure 21 the permittivity of water is given using data for calibration measured without the foil. In this case there is a systematic error since the effect of foil is in the measured data but it hasn't taken under consideration in calibration.
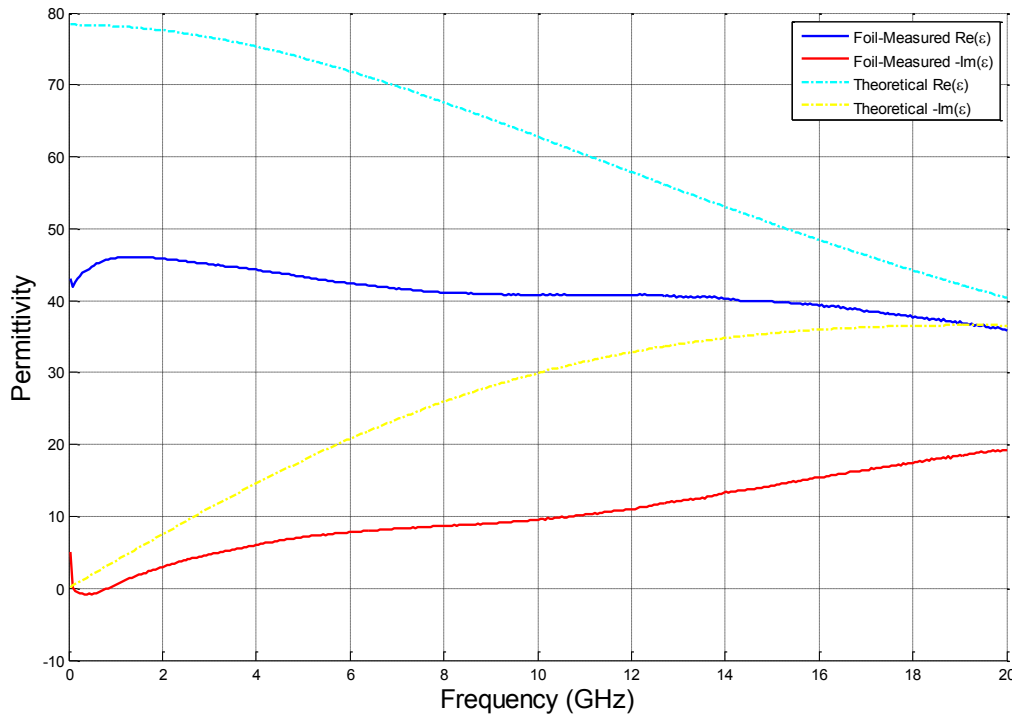
Figure 21. A measurement for water using the plastic foil on the probe but calibration data measured without the foil. The systematic error is obvious.

5.2 Experiments with rectangular waveguides

At this part of this Thesis a rectangular waveguide completely or partially filled with an epoxy slab has been examined, in order to measure its permittivity and permeability using the NRW algorithm.

5.2.1 Filled Waveguide

Firstly the filled rectangular waveguide was simulated with the Comsol Multiphysics program. The results were compared with the measured data from experiments of Daniel Sjöberg and Christer Larsson [Private Communication]. The material parameters of epoxy, as they used for simulations, are $\varepsilon_r = 2.8 - 0.015j$, $\mu_r = 1$ and $\sigma = 0$.

Two epoxy slabs were measured, one with thickness 9.61 mm and one with 5.11 mm. The waveguide is a WR-90 X-band with cutoff frequency 6.56 GHz designed for the frequency range 8.2-12.4 GHz [Damaskos Inc, Sjöberg and Larsson 2011]. The measure frequency interval is 6.6-12.9 GHz. For the measured data the TRL calibration method was used [Engen and Hoer 1979]. The operating mode is TE_{10}.

35

The measurement setup consisted of a network analyzer connected to two waveguide segments, joined by a sample holder containing the sample under test. Here the importance of the sample holder has to be emphasized, where without it there are no line and reflect standards. The reflect standard is a short that is given by the manufacturer together with the sample holder.

In the photos in Figure 22 are shown the sample holder filled, the epoxy slab, the short standard and how the sample holder is connected to the two waveguides.

a.   b.
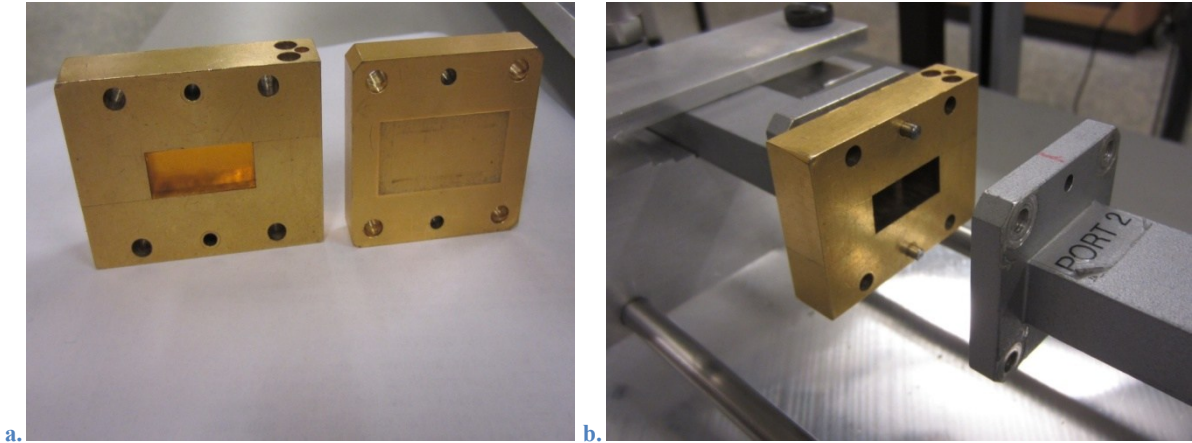
Figure 22. a. The sample holder filled with a sample and the short standard, b. The sample holder placed on the rectangular waveguide.

In Figure 23 the 9.61 slab as designed with the Comsol Multiphysics is presented.
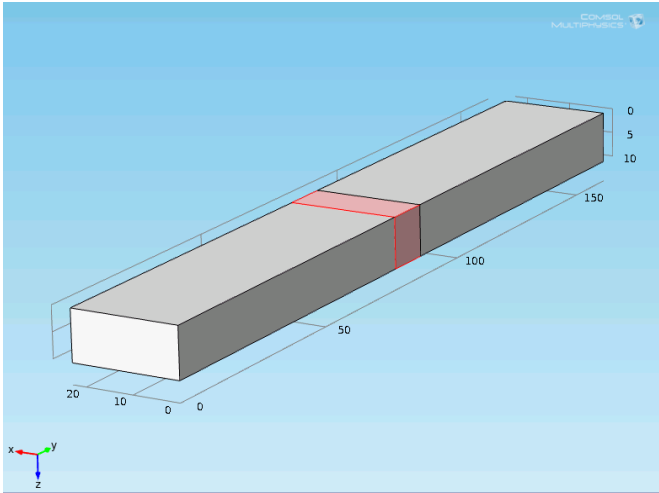
Figure 23. A rectangular waveguide filled with a sample designed with the Comsol Multiphysics program.

At this part of the Thesis the diagrams from the Transmission/Reflection Experiments are given. In Figures 24 and 25 comparisons among measured and simulated data for the 9.61mm slab are shown. For the simulations the electromagnetic parameters of the sample are assumed to be $\varepsilon_r = 2.8 - 0.015j$ and $\mu_r = 1$.
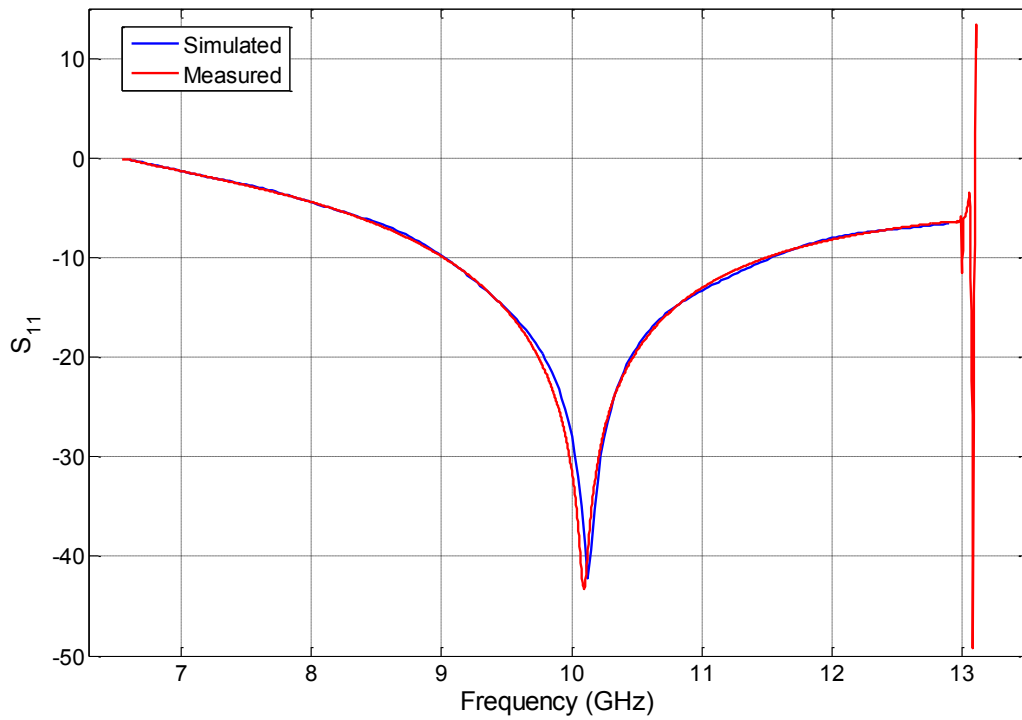
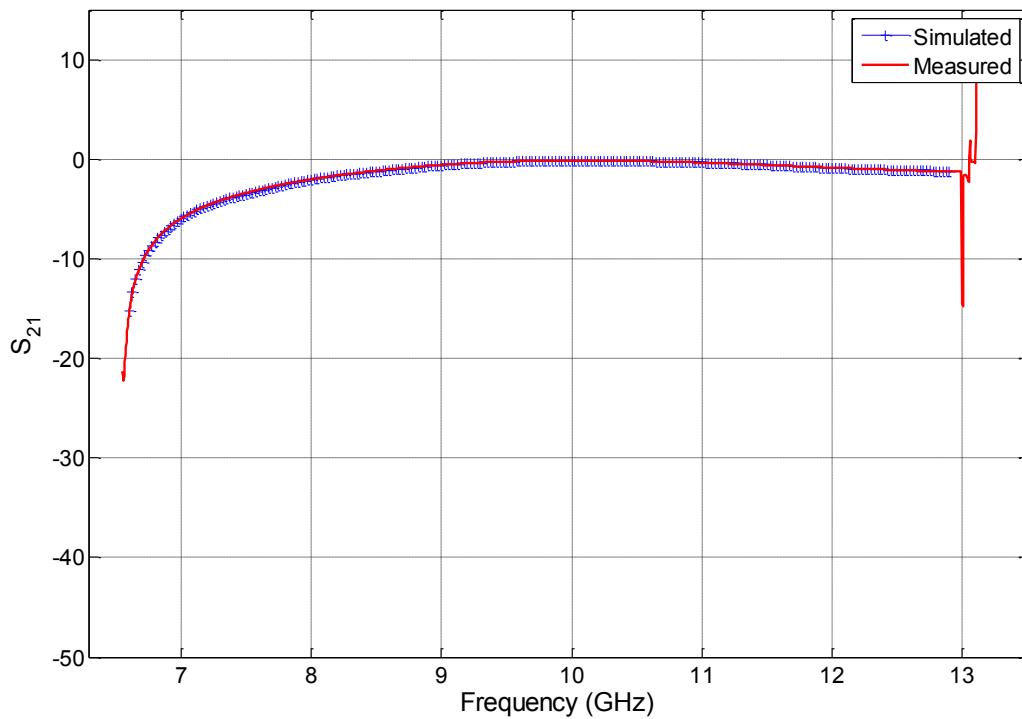**Figure 24. S$_{11}$ from simulation and measurement.**

Figure 25. S$_{21}$ from simulation and measurement.

In Figure 24 the S$_{11}$ for both cases is shown. It begins from zero at 6.6 GHz and decreasing until 10.13 GHz where takes its minimum value -42.5 dB ant then increases logarithmically

until -6.5 dB at 12.86 GHz. At 10.13 GHz all the electromagnetic field is propagating through the slab. This behavior of the half-wavelength thick slab is the behavior of a band pass microwave filter. This is also shown in the Figure 25 of S_{21} against frequency.

The S_{21} begins at -15 dB and increases until 10.1 GHz where it becomes zero and then increases a little until -1.25 dB at 12.9 GHz.

Both the measured results and the simulated ones agree with the calculations of the mathematical equations which describe this phenomenon. These data can be used as input for the NRW algorithm to determine the electromagnetic parameters of the sample.

In Figure 26 some views of the electromagnetic field are given. The electric field norm $\left(\frac{V}{m}\right)$ at 10 GHz is shown. At the part before the sample at the propagation axis (y at these photos) concentrations and dilutions can be observed. Theses concentrations and dilutions are due to the superposition of the transmitted and reflected wave at this part of waveguide. At the part after the sample there is only the transmitted wave. The electric field norm is maximum around the propagation axis of the waveguide and zero at the walls of the waveguide. In Figure 26a one can see the wave at the plane *xy* and in the Figure 26b the wave at the *yz* plane.
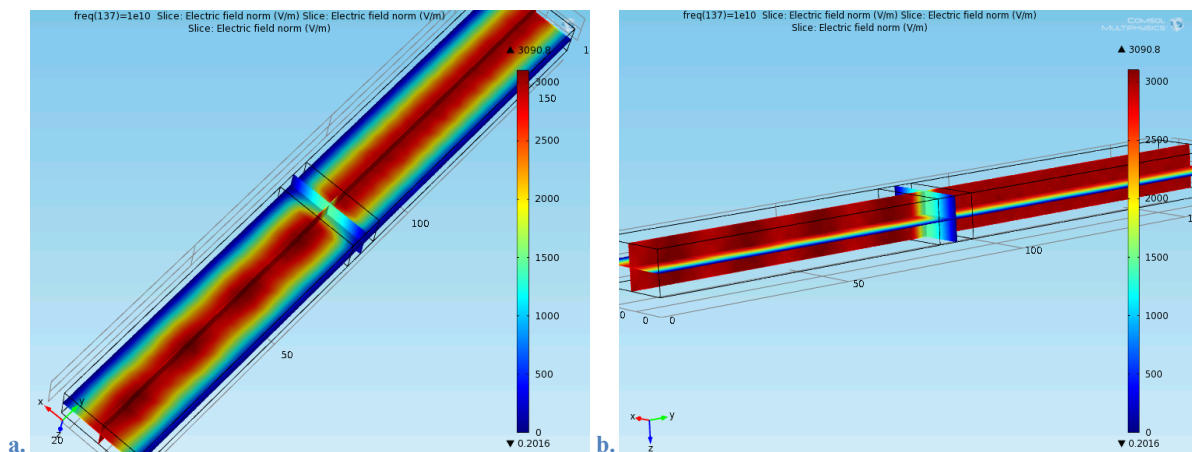

Figure 26. The electric field norm at 10 GHz inside the waveguide a. at the *xy* plane, b. at the *yz* plane.

A view of the electromagnetic field (electric field norm) at 6.6 GHz is shown in Figure 27a. This is the lowest frequency value used here. It is seen that the wave does not propagates inside the waveguide.

In Figure 27b a view at 9 GHz is given. Here the concentrations and dilutions are very intense and the electric field norm is around 4000 $\left(\frac{V}{m}\right)$ at the center of the y axis while at the other side of the sample at the same axis the norm is lower, around 3000 $\left(\frac{V}{m}\right)$. This means that the bigger part of the wave is reflected at the sample and only a little part is transmitted through it, high S_{11} and low S_{21}.
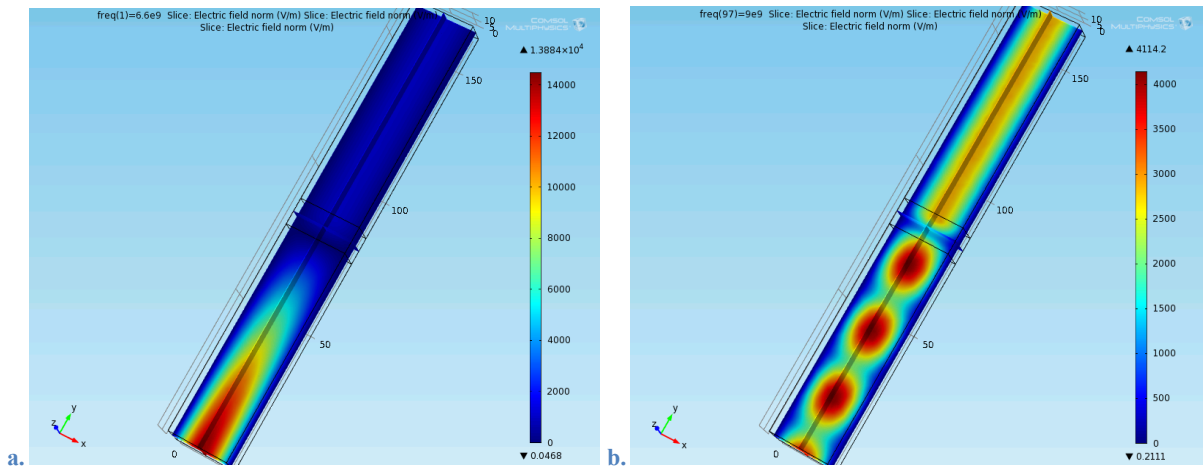
Figure 27. The electric field norm inside the waveguide a. at 6.6 GHz, b. at 9 GHz.

A view of the propagating electromagnetic wave at 10.125 GHz is shown in Figure 28. At this frequency all the wave is transmitted through the sample and practically no wave is reflected back. The S_{11} is minimum (-42.25 *dB*) and the S_{21} (0 dB) is maximum and the electric field norm is the same at the two sides of the sample.
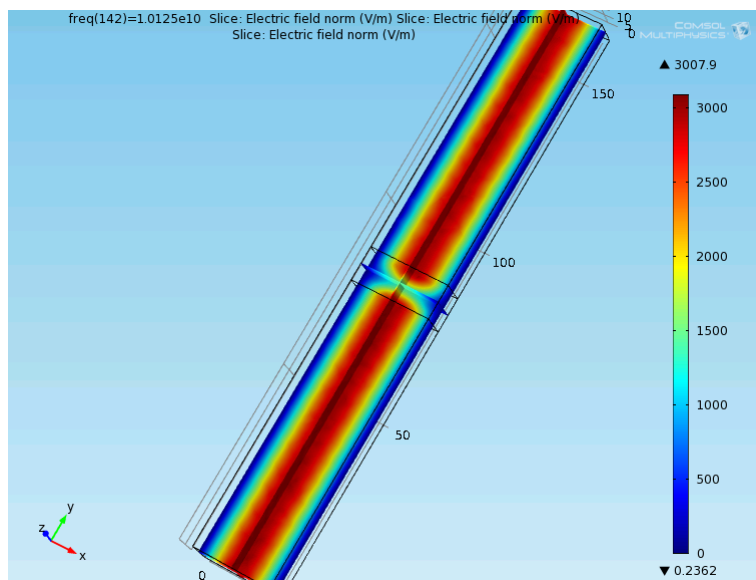

Figure 28. The electric field norm inside the waveguide at 10.125 GHz.

In Figures 29 and 30 the transmission and reflection coefficients of the rectangular waveguide filled with the 5.11mm slab are shown. This sample is shorter than a half-wavelength in the whole frequency band and so the behavior of the scattering parameters is different than that of a band pass filter. The S_{11} start from zero and smoothly decreases until 12.9 GHz where it has its minimum value of -6.8 dB. In the simulated data a slight ripple exists and there is a little difference between the simulated and the measured coefficient. Similarly the transmission coefficient is increasing smoothly from -13.77 dB at 6.6 GHz up to -1.1 dB at 12.9 GHz. Here there is no perfect transmission of the wave through the slab but always there is a part that is reflected.
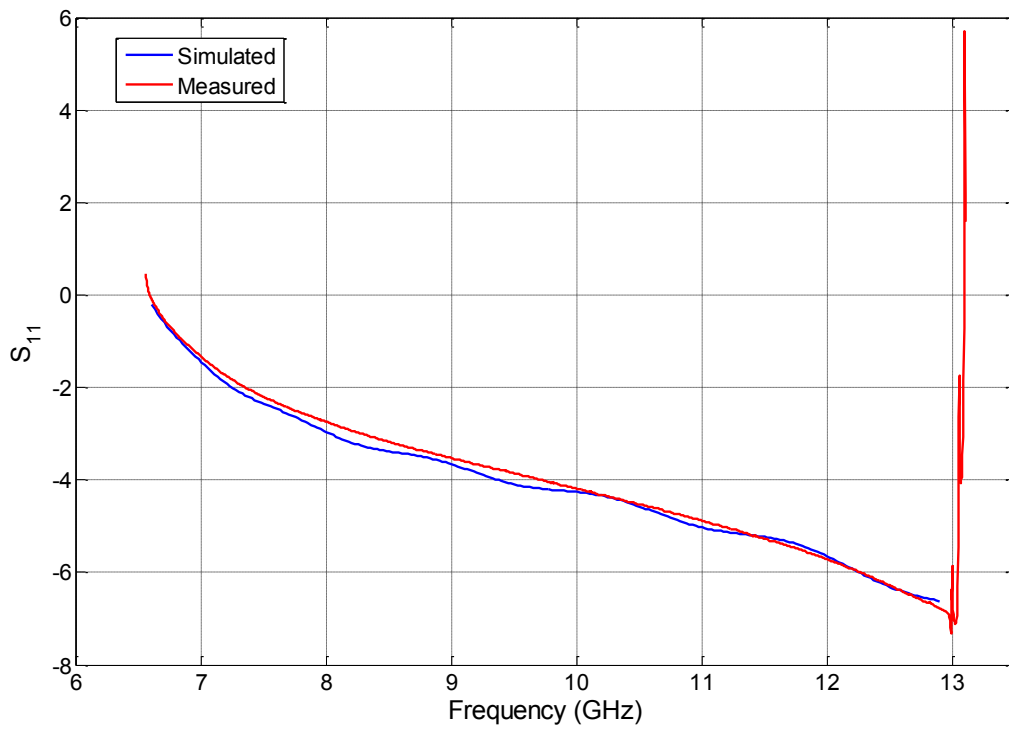
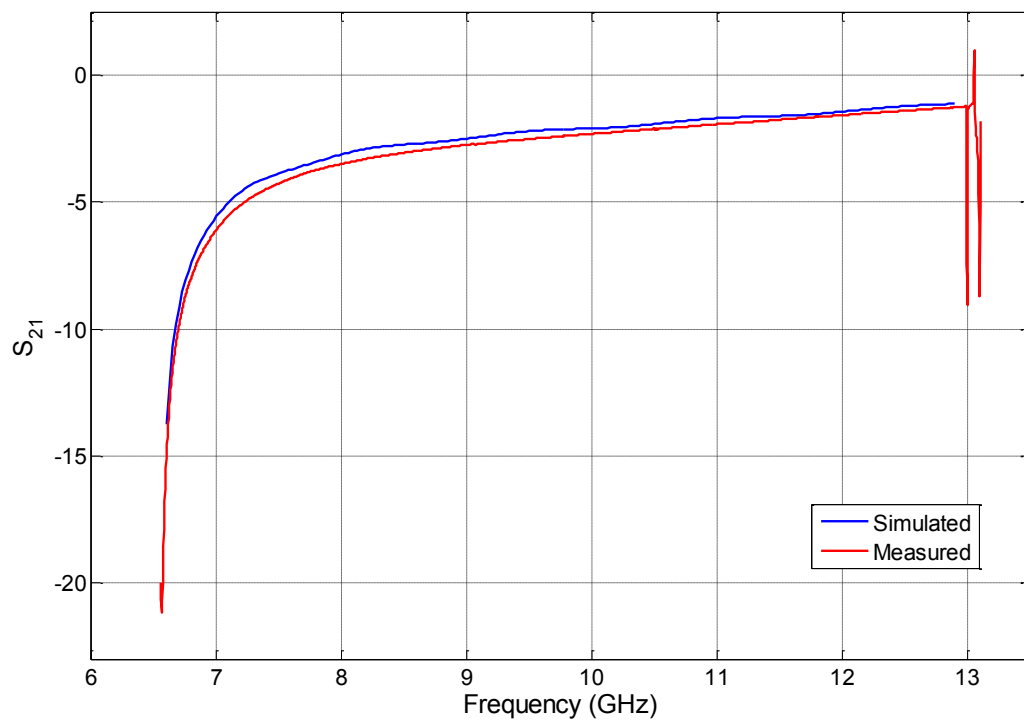**Figure 29. S₁₁ from simulation and measurement on the 5.11mm slab.**

Figure 30. S₂₁ from simulation and measurement on the 5.11mm slab.

5.2.2 **Partially Filled Waveguides**

In this part of this Thesis all the possible cases of the waveguide partially filled with the 9.61 slab was simulated and some of the data extracted were compared with some measured and calibrated data. The 5.11 slab is too small to partially fill the waveguide and out of the scope of this work.

The first case (Case A) is shown in Figure 31a where the slab is turned 90° around the x axis. In Figure 31b the case B is shown where the sample after the 90° turn around the x axis is also turned 90° around the z axis.
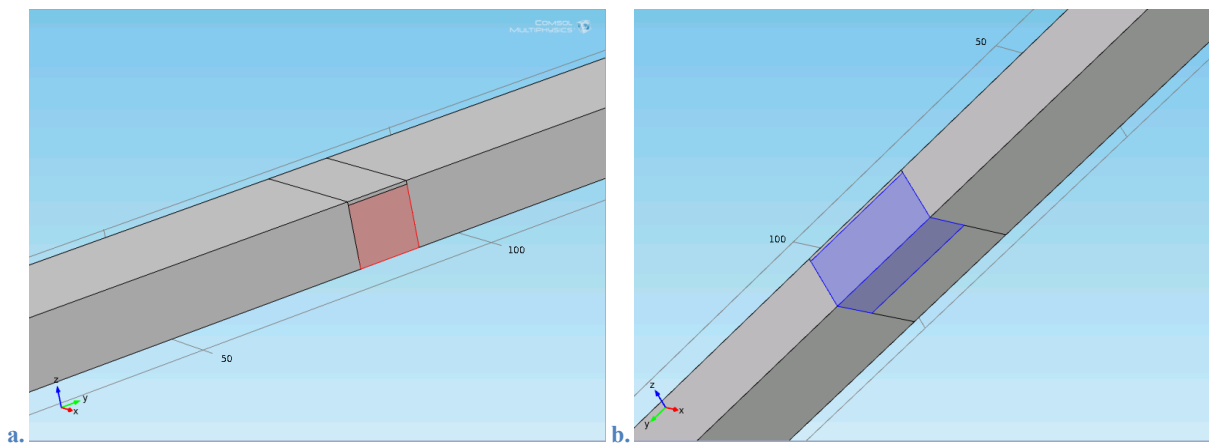

Figure 31. Two different cases of partially filled waveguides a. Case A, the slab is turned 90° around the x axis, b. Case B, the slab is additionally turned 90° around the z axis. Note the small air gap between the slab and the waveguide at the top.

In the B2 case (Figure 32) the slab is turned around x and z axis and also moved at the center of the waveguide. For this case there are no available measured data.
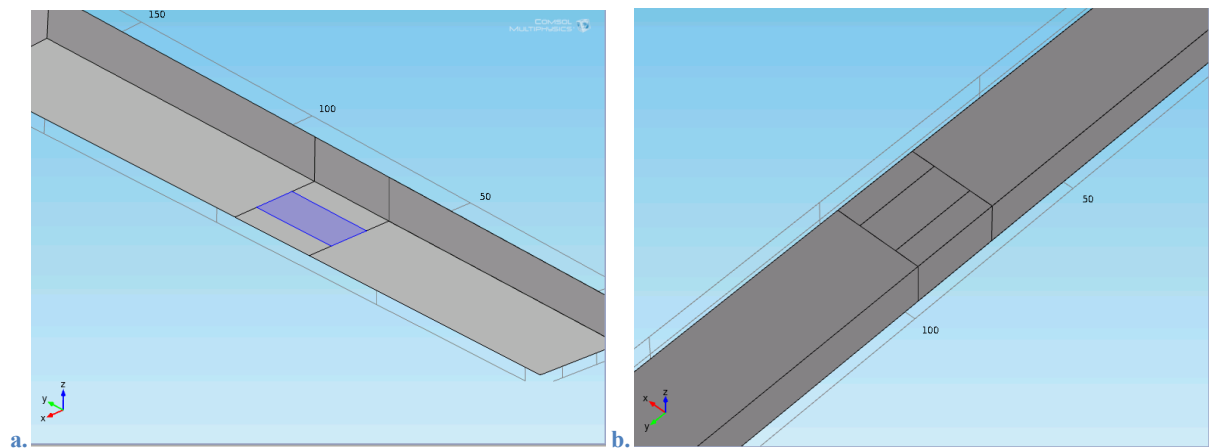

Figure 32. Partially filled waveguide, Case B2, the axis of the sample is parallel to propagation axis and between its upper side and the waveguide there is an air gap, a. bottom view, b. upper view.

In the Figure 33a the case C is presented, the slab from the original filling the waveguide position has turned directly around the z axis. A view of the electromagnetic field propagating in the waveguide for this case is given in Figure 33b. The wave propagates in the epoxy slab

41

and not in the air gap, since the epoxy has dielectric constant 2.8 while the air 1. In the slab transmitted and reflected wave propagates and the superposition is clear. This image illustrates the principle shown in Figure 5.
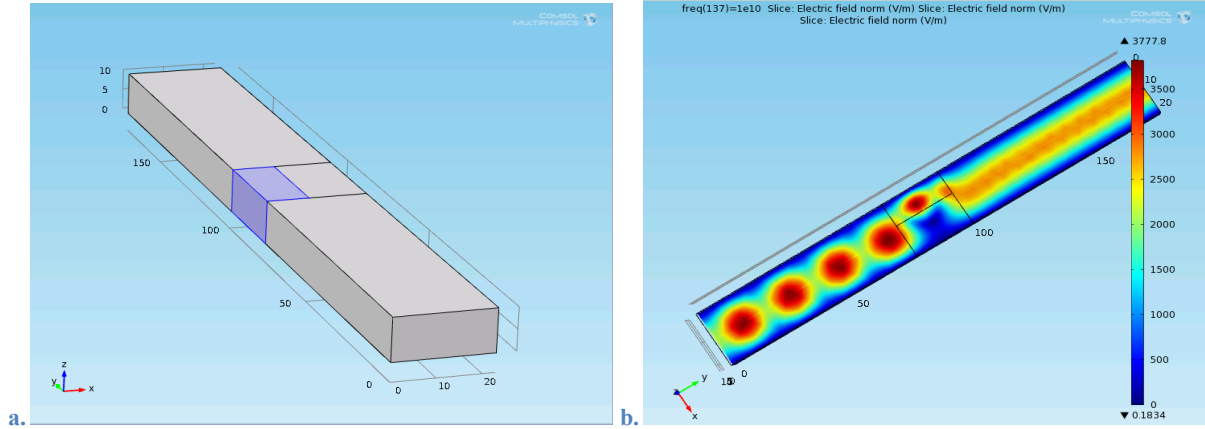

Figure 33. A partially filled waveguide, the sample is placed at the side of the waveguide (Case C), a. A view of the sample in the waveguide, b. The electric norm in the waveguide.

Similarly the case C2 where the slab after the turn around the z axis has moved also at the center of the waveguide is shown in Figure 34 and respectively an image of the electromagnetic wave in the same figure. Here the electromagnetic field propagates also in the sample for the same reasons as previously only but in more narrow space.
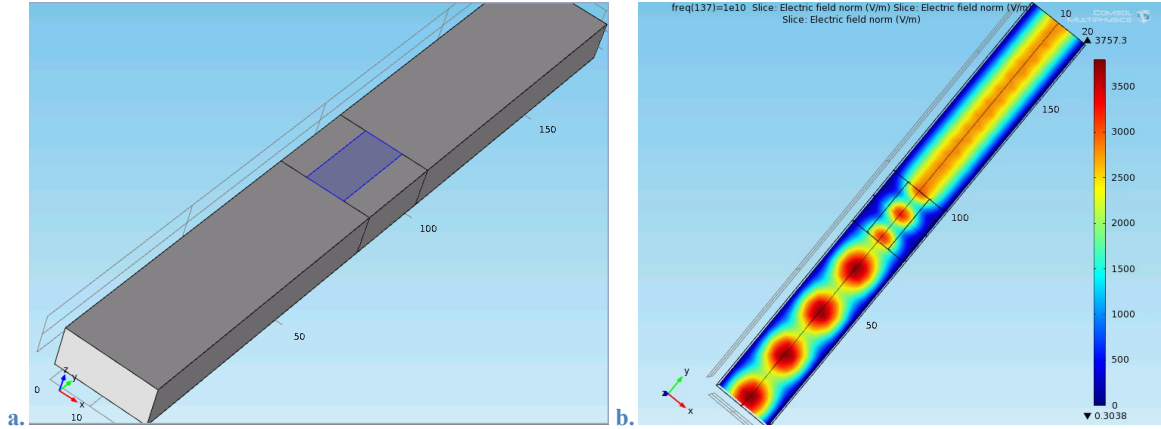

Figure 34. The Case C2 of the partially filled waveguide, a. A view of the sample in the waveguide and b. The electric norm in the waveguide.

5.2.3 Results of the Transmission/Reflection Experiments

Following, the phase against the frequency is given. At the simulated data there is the problem of phase ambiguity. The phase changes between $+\pi$ and $-\pi$. This happens because the measuring ports are at the edges of the waveguide (planes 1 and 2) and not at the edges of the sample (planes 3 and 4) (Figure 6). For the magnitude of S parameters there is no difference but for the phase there is. So the planes have to be transferred from the planes 1, 2 to the planes 3, 4 in order to measure S_{33} and S_{34}. A plane transfer has presented by Larsson,

Sjöberg and Elmkvist [Larsson *et al.* 2011] and this method has been used here to transfer the planes for the simulated data, Figure 35.
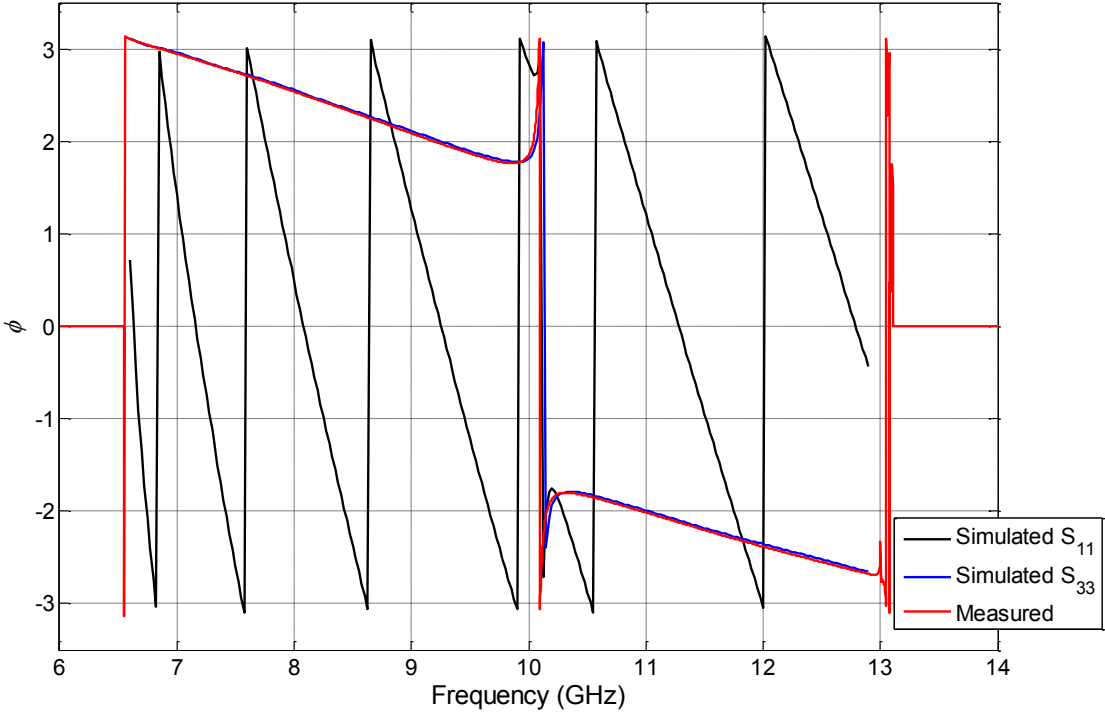

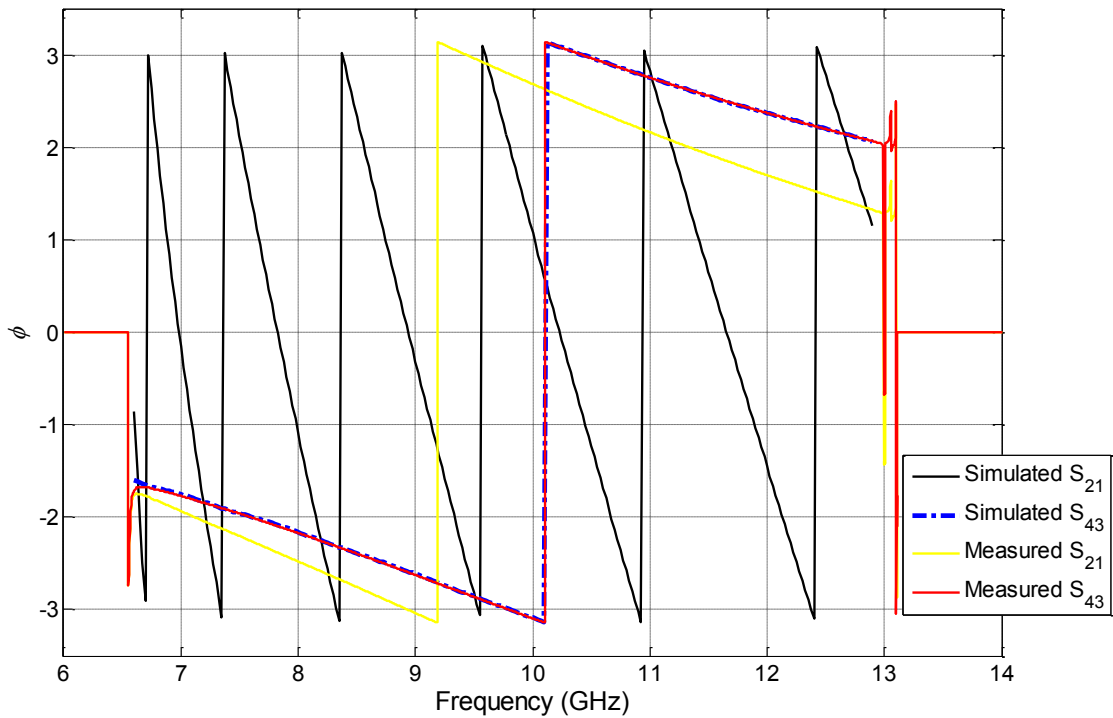**Figure 35. The phase of S₃₃ for measured data is the same as S₁₁ but the simulation results needs to be transformed.**

Figure 36. The phase of S₄₃ for all the available data. For the data from the simulation and the measurement needs to be transformed from S₂₁.

In Figure 36 is presented the transfer of the transmission coefficients for the measured data and the simulation results. The scattering parameters S_{21} has transformed to S_{43}.

Continuing, the evaluation of available data with the Nicolson Ross Weir algorithm takes place in order to determine the electromagnetic properties of the sample. In the Figures 37 and 38 the permittivity and the permeability of the epoxy are shown after evaluating all the data (measured and simulated) for the 9.61mm sample.
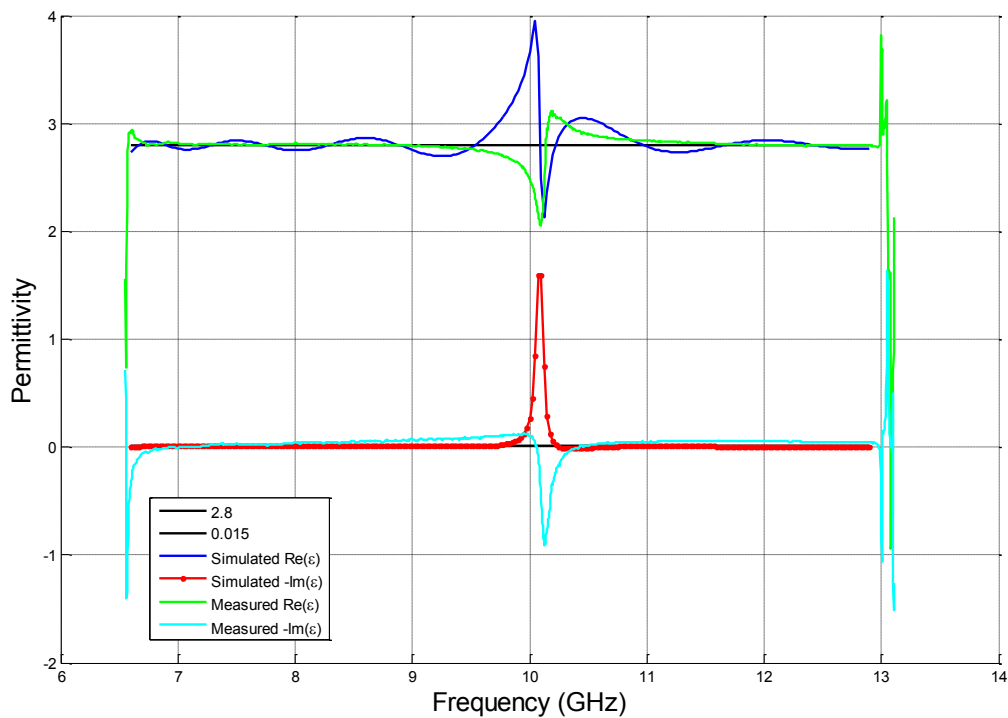
Figure 37. Epoxy permittivity after the evaluation of all the available data from 9,61mm slab with the NRW algorithm.

It is clear that at 10.13 GHz the values of the electromagnetic parameters have an unexpected peak for the measured especially but also for the simulation's data.

For the permittivity (Figure 37) below 10.13 GHz the dielectric constant of the permittivity (real part) according the measured data is 2.8, ignoring the instability at 10.13 GHz. From 9.7 to 10.8 GHz, the dielectric constant is different than 2.8, and specifically around 10.13 GHz takes values from 2 to 3.1. Above 10.8 GHz the permittivity is 2.8.

In the resulting permittivity from the simulation's data there is inconsistency at 10.13 GHz but the values are close to the real ones especially for the loss factor. At the permittivity constant a ripple is observed and gives values from 2.7 up to 3.

As for the permeability (Figure 38) the measured data give value 1 from 6.6 up to 9.8 GHz and from 10.3 up to 13 GHz, and for a nonmagnetic material is expected $\mu = 1$. Around 10.13 GHz the permeability takes values between 1.3 and 0.9. The loss factor is 0 as is expected, except the frequencies around 10.13 where the instability exists and results a value of 0.4.

The simulation's data give similar results. The ripple at the permeability is between 1.035 and 0.92.
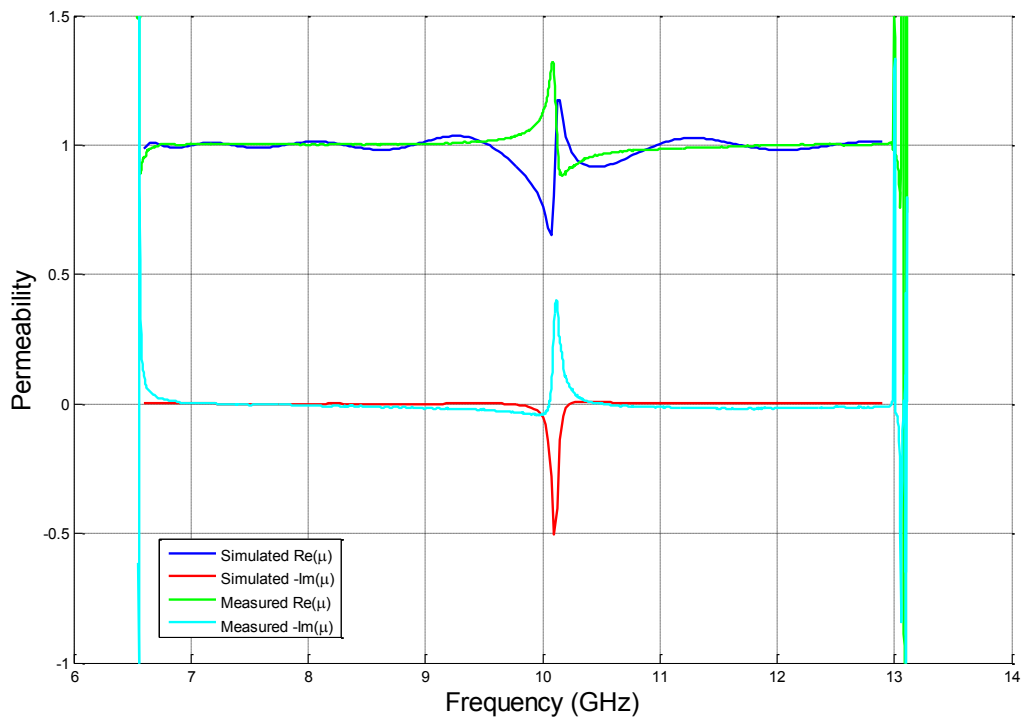
Figure 38. Epoxy permeability after the evaluation of all the available data from 9,61mm slab with the NRW algorithm.

At the measured results some oscillations can be observed. To have more smooth curves the reflection coefficient from the right side (S_{22}) can also be used and by taking the geometrically mean of S_{11} and S_{22} these oscillations can be avoided.

To avoid this instability the permeability can be settled to 1 ($\mu = 1$), Figure 39.

The measured data give perfect results and the simulations much better than before. The simulated results have a slight but ignorable ripple up to 7.4 GHz.
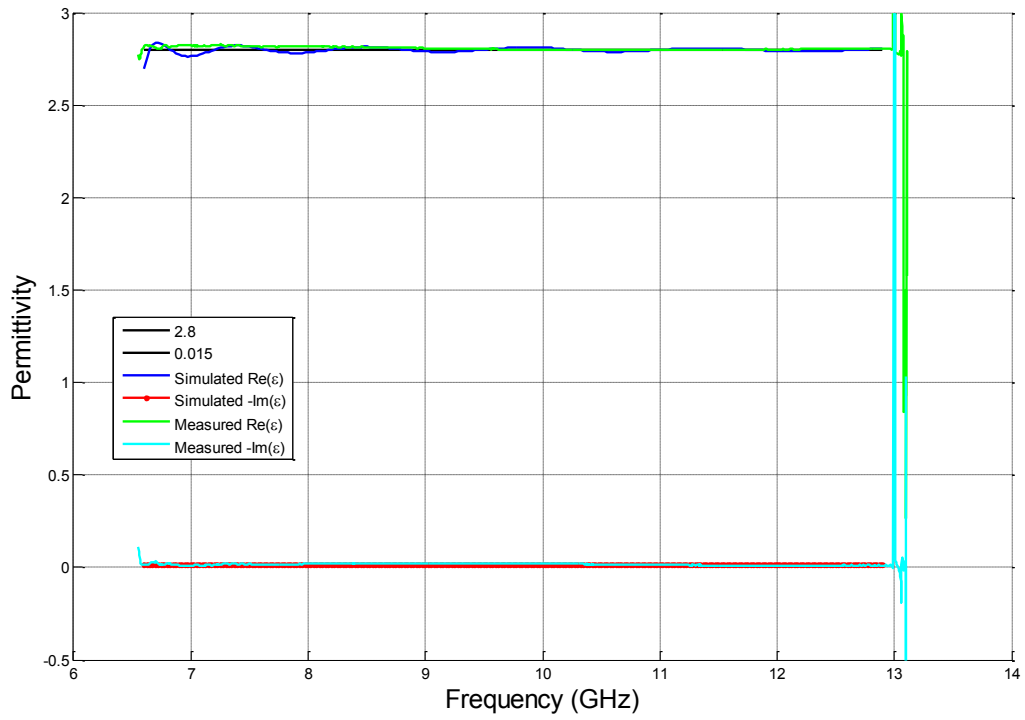
Figure 39. Epoxy permittivity after the evaluation of all the available data from 9,61mm slab with the NRW algorithm and by setting permeability equal to 1 ($\mu = 1$).

The evaluation of the results for the 5.11mm sample is given in Figures 40 and 41.
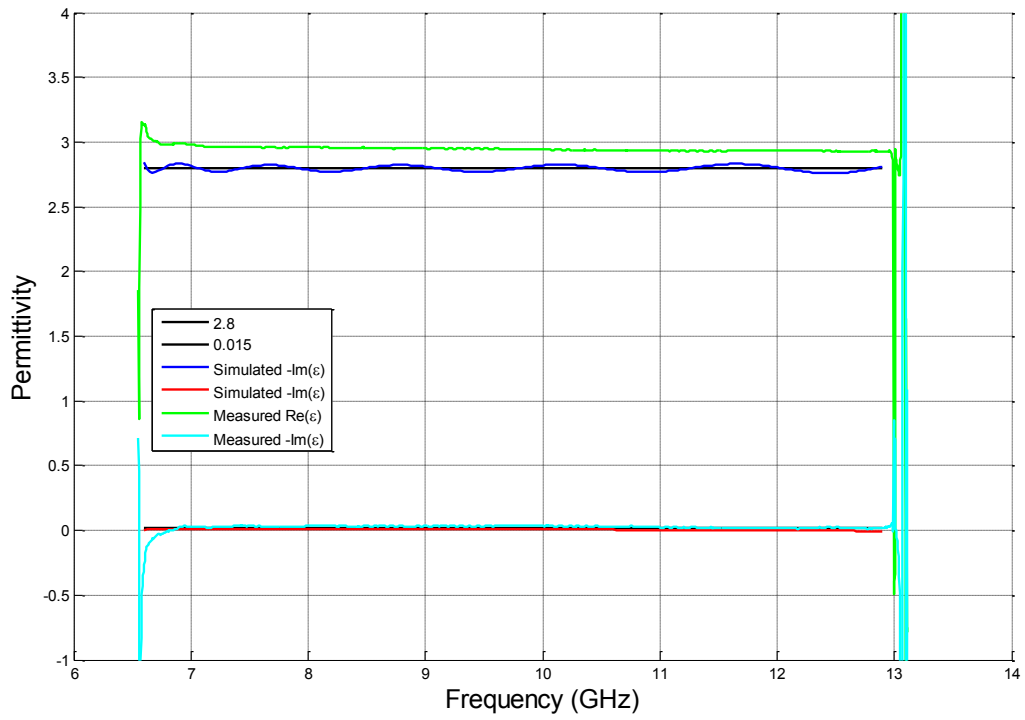
Figure 40. Epoxy permittivity after the evaluation of all the available data from 5,11mm slab with the NRW algorithm.
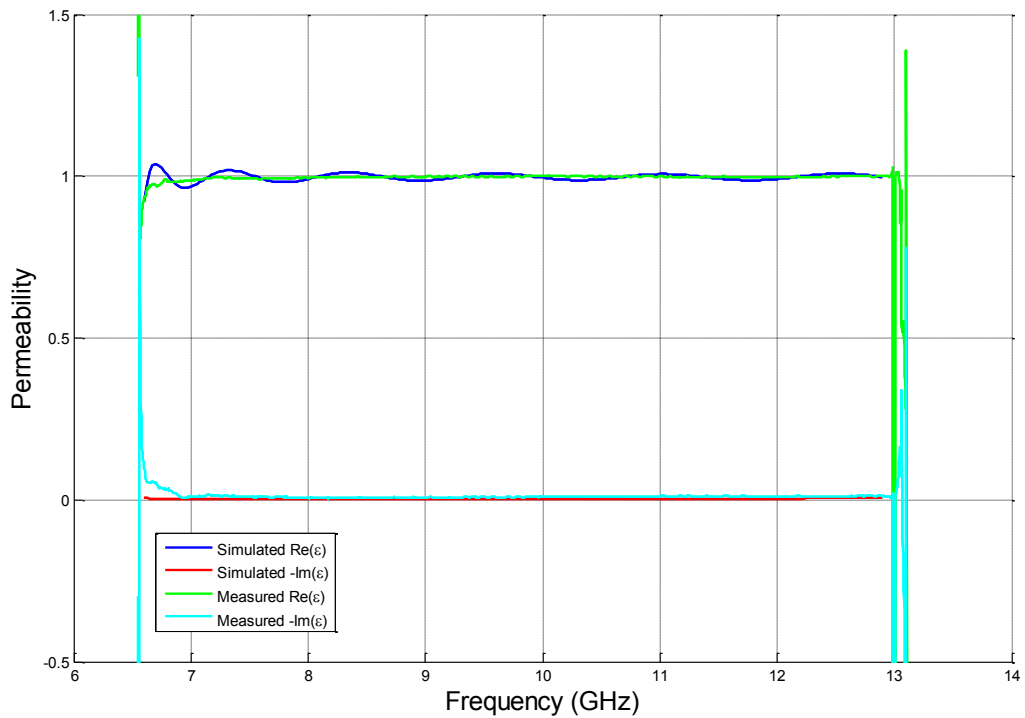

Figure 41. Epoxy permeability after the evaluation of all the available data from 5,11mm slab with the NRW algorithm.

Here there is no peak at 10.13 GHz. The data from the simulation again give a ripple especially in the permeability. The difference between the measured and simulated results is due to the permittivity of this sample. For the simulations the same value as before was used ($\varepsilon = 2.8 - 0.015j$) but the real value of this sample's permittivity is the one that is shown here, $\varepsilon = 2.9 - 0.03j$.

The sample's permeability is $\mu = 1$. The measurements give perfect results but the simulations again a ripple.

By setting the permeability to one ($\mu = 1$) (Figure 42) the resulting permittivity is $\varepsilon = 2.9 - 0.05j$. This value is more correct since the algorithm is more stable after the assumption of non magnetic sample.
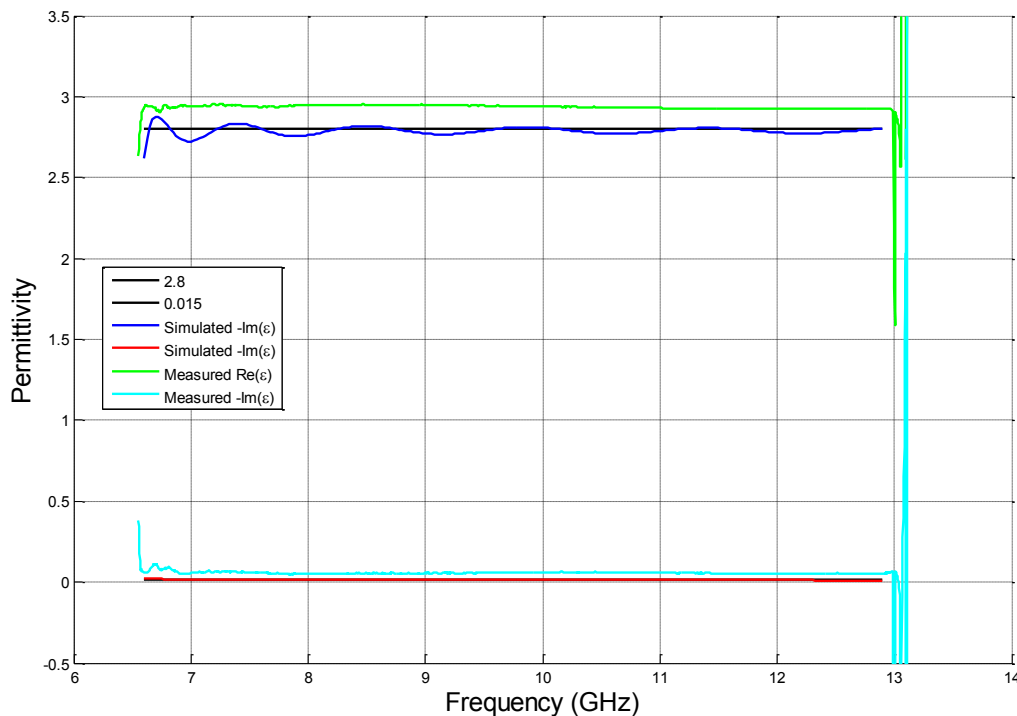

Figure 42. Epoxy permittivity after the evaluation of all the available data from 5.11 mm slab with the NRW algorithm and by setting permeability equal to 1 ($\mu = 1$).

The problems at frequencies below 7 GHz for the measured data are due to the fact that WR-90 waveguides are designed to operate at frequency range 8.2-12.4 GHz.

Considering the conclusions of Sjöberg and Larsson (Sjöberg and Larsson 2011) one can conclude that there is no problem on the algorithm but the problem is in the data and especially when the sample has thickness of half-wavelength. On the other hand, since these data give correct scattering parameters the problem can be found in how these data function in NRW, namely what is in the nature of these data that result the problem.

In the Figures 43-47 the reflection scattering parameter S_{11} of the data from the partially filled waveguides are given. The Comsol Multiphysics Models are seem to work very well and can extract very trustable data.
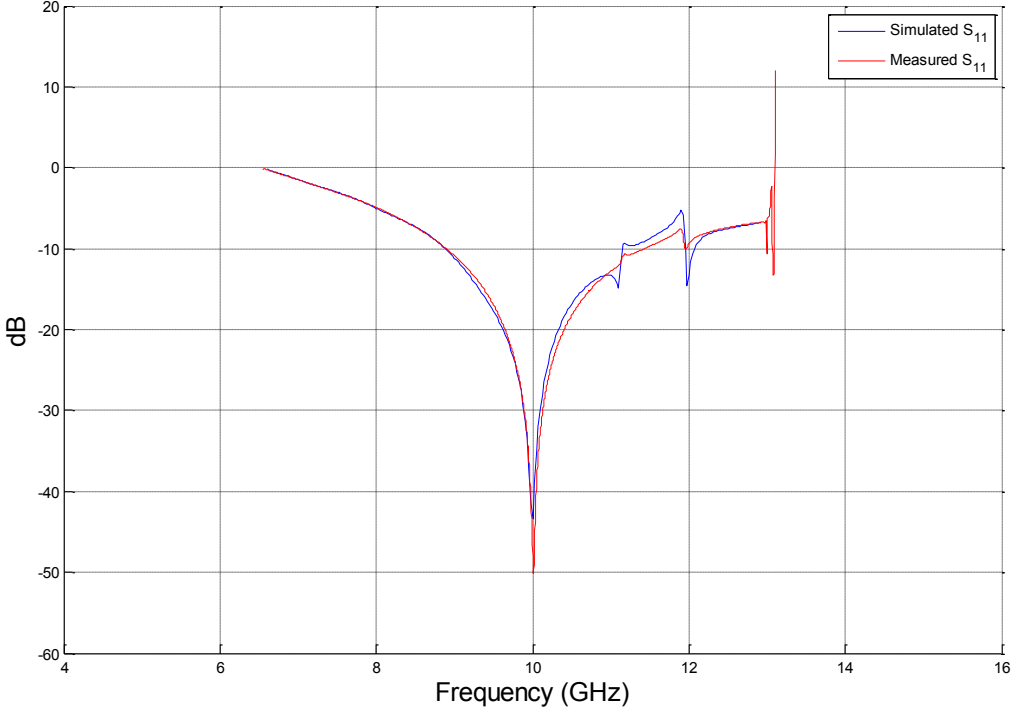

Figure 43. S_{11} from simulation and measurement on partially filled waveguide, Case A.

In Figure 43 the reflection coefficient for the case A is shown. At 10 GHz the entire electromagnetic wave propagates and there is no reflection. Between 11 and 12 GHz some peaks are shown in the curves due to the small air gap between the sample and the top of the waveguide. These results can be used in NRW algorithm and give some notable results.

In Figure 44 the reflection of the case B is shown. The wave is primarily transmitted at 7, 11 and 12.3 GHz. The peaks between 11 and 12 GHz can be occurred from the existence of high order modes.

The mismatches between data in Figures 43 and 44 can be due to mechanical problems in fitting the sample in the waveguide or limitations of Comsol Multiphysics.
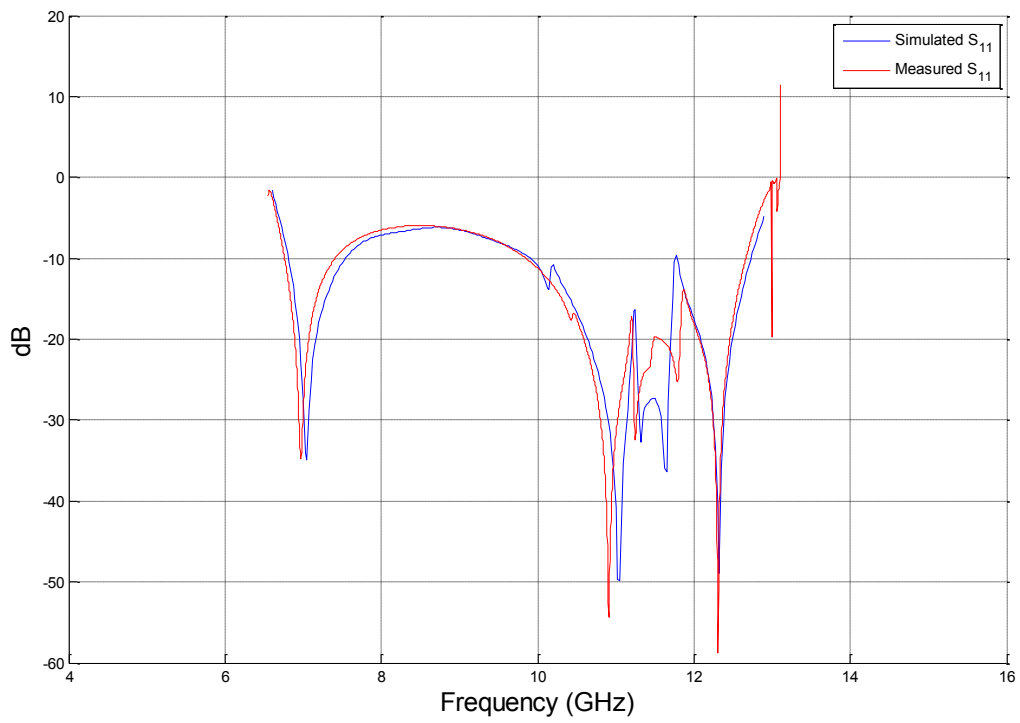
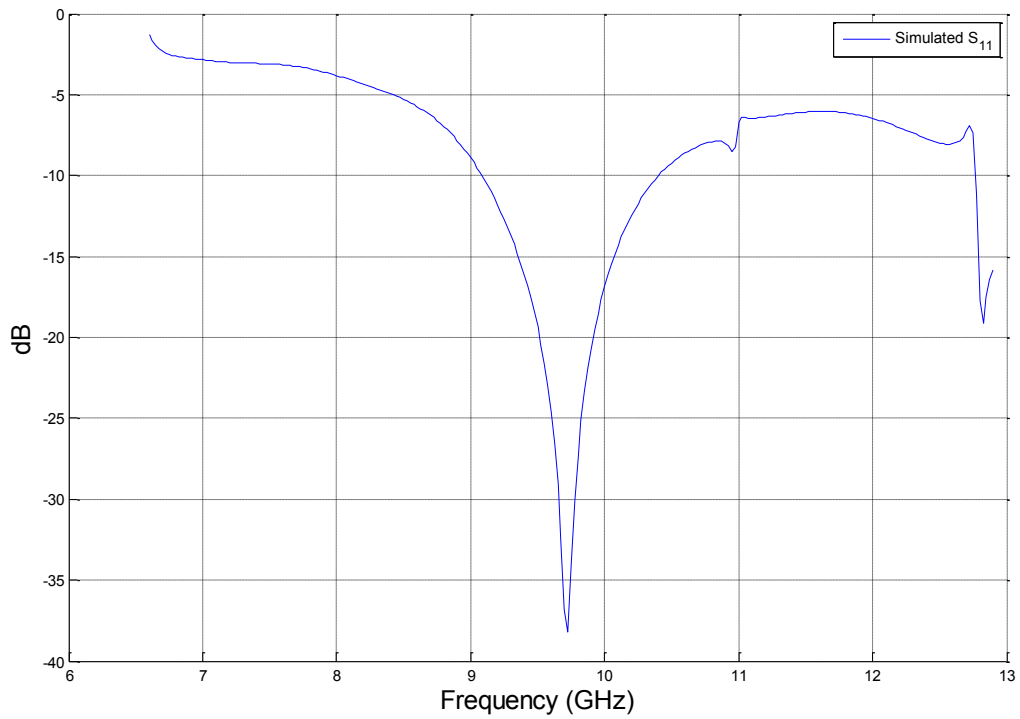Figure 44. S$_{11}$ from simulation and measurement on partially filled waveguide, Case B.

Figure 45. S$_{11}$ from simulation on partially filled waveguide, Case B2.

The scattering parameter S_{11} for the B2 is shown in Figure 45. The sample is centered in the waveguide. The electromagnetic wave mainly propagates at 9.7 GHz. Some peaks exist around 11 and 12.8 GHz.

In Figure 46 reflection coefficient from the case C is shown. The electromagnetic wave mostly is reflected from 7.5 to 10 GHz and mostly transmitted at 7, 10.93 and 12.2 GHz and there are a few similarities with the case B.

A very interesting case for a partially filled waveguide is the case C2 and the S_{11} for it is shown in Figure 47. The curve is very smooth with minimum at 9.475 GHz where the electromagnetic wave has an almost perfect transmission through the sample. This case was used for determination of the complex permittivity (Catalá-Civera *et al.* 2003) and using algorithm different than NRW can give some good results.
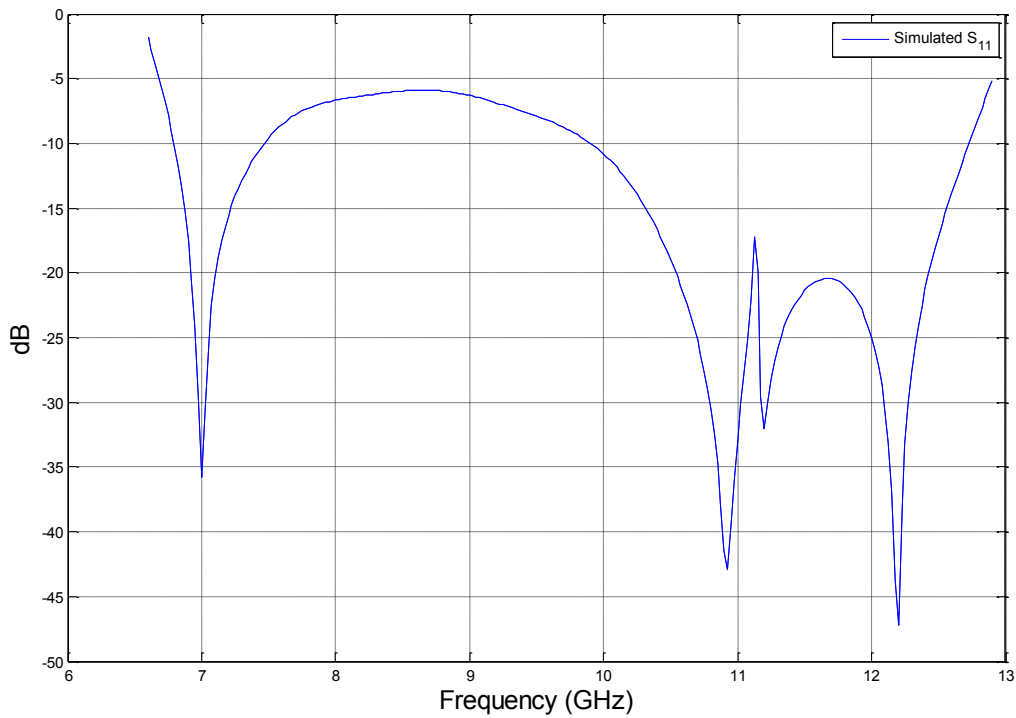

Figure 46. S_{11} from simulation on partially filled waveguide, Case C.
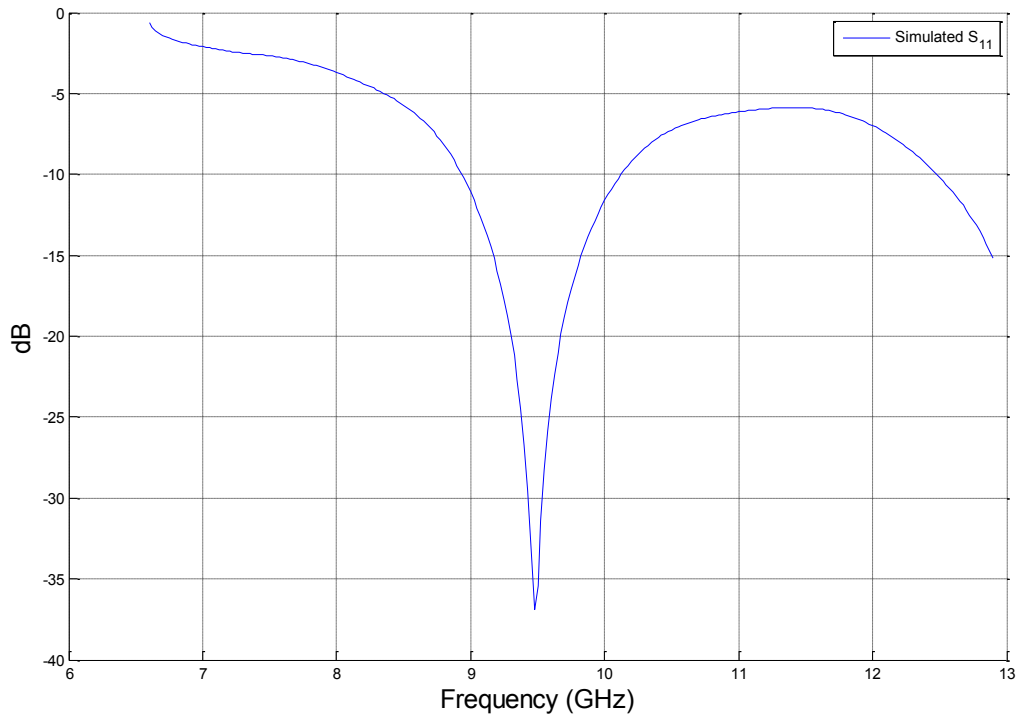
Figure 47. S_{11} from simulation on partially filled waveguide, Case C2.

5.2.4 **NRW and Partially Filled Waveguides**

The data from partially filled waveguides cannot be evaluated using the NRW except the case A. In the case A the air gap between the sample and the waveguide is small and the electromagnetic parameters can be derived with the difference of the real ones described in Equations (4.20), (4.21).

The resulting parameters after using the data from the Comsol Multiphysics simulation of case A and the corresponding measured are shown in Figure 48. The permeability has been defined 1 ($\mu = 1$). The peaks at 11.13 and 11.93 GHz are due to the air gap. These peaks are much higher for the simulations than the measurements which mean that the measured data are more accurate. The inconsistency at frequencies below 9 GHz is due to the instability of the implementation which can be avoided by using the S_{44} additionally.

The measured permittivity by observing Figure (48) is approximately $\varepsilon_m = 2.6 - 0.013j$. By using the Equation (4.20) with $\varepsilon_s = 2.8 - 0.015$, $\varepsilon_g = 1$, $b_s = 9.61$ mm and $b = 10.16$mm the measured permittivity is calculated $\varepsilon_m = 2.55 - 0.0118j$ which is very close to the value above.
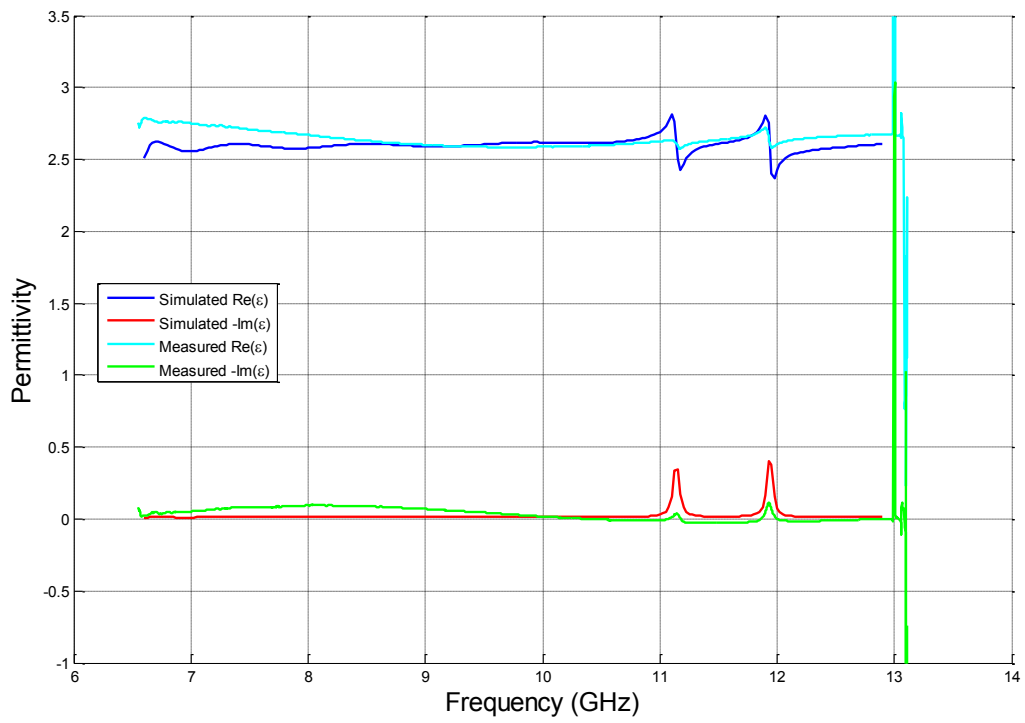
Figure 48. Epoxy permittivity after the evaluation of all the available data from partially filled waveguide (Case A) with the NRW algorithm by setting permeability equal to 1 ($\mu = 1$).

The evaluation with NRW of the data from the simulation cases B2 and C2 are shown in Figure 49.
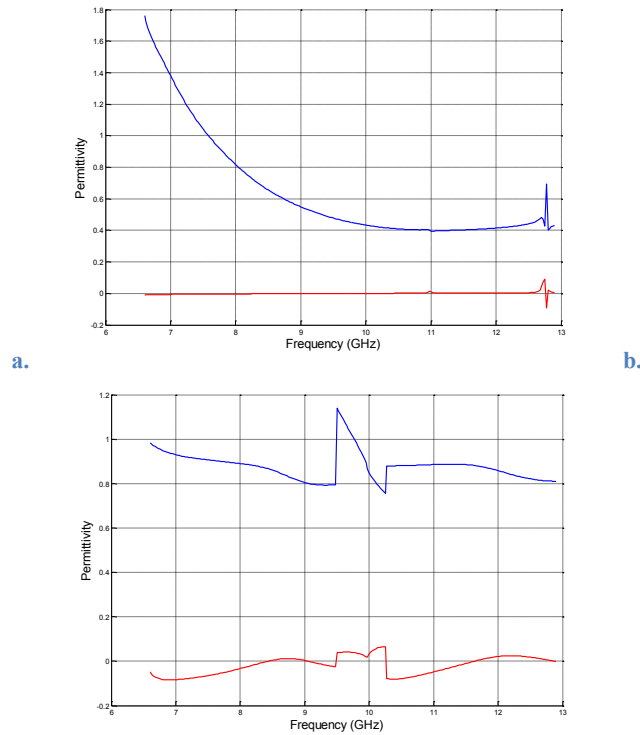
Figure 49. Some results from NRW when using as input data from partially filled waveguides, a. Case B2 and b. Case C2.

Figure 49 clearly shows that the NRW cannot be used on partially filled waveguides to determine the electromagnetic parameters, permittivity and permeability. It was shown in this Thesis that full wave simulations can produce scattering parameters similar to the measured parameters even for partially filled waveguides. Thus, an optimization algorithm could be devised, where the permittivity used in the simulation is changed until the S-parameters of the simulation match the S-parameters of the measurement.

6. Conclusions

A reflection and a transmission/reflection method have been used in this Thesis to determine the electromagnetic parameters of some materials. The reflection method to determine the permittivity of some deep enough liquid and solid samples and the transmission/reflection method was used to determine both the permittivity and permeability of some slabs.

With the coaxial probe modeled as antenna and calibrated using four known standards the permittivity of saline, isopropyl alcohol, Rohacell, EPS, wood and rubber was determined over a frequency range 0-20 GHz.

This procedure is working very well and mostly for liquid samples where the air gaps can be eliminated and the probe can perfectly touch the sample. In this respect it is suitable for "in vivo" measurements.

As for the methods using partially filled waveguides it has been clearly presented that Comsol Multiphysics can simulate with high accuracy the filled and partially filled rectangular waveguides and the measuring process is also of the same quality.

Nicolson-Ross-Weir algorithm can determine complex permittivity and permeability from scattering parameters from filled waveguides but some parameters must be taken into account. The data -rather the NRW algorithm- cannot give good results when half-wavelength samples are measured. At frequencies where the sample length is a multiple of half wavelength in the material there are abnormalities on resulting parameters. At these frequencies there is no reflection data but only transmission, and regarding that a Transmission/Reflection method to work needs both the transmission and reflection coefficients to derive two parameters – permittivity and permeability-, one can conclude that at these frequencies the Transmission/Reflection method becomes only Transmission method and thus can derive only one parameter.

For the partially filled waveguides NRW algorithm does not work and other algorithms must be used to determine the electromagnetic parameters. But still NRW can give notable results when the air gaps between the sample and the waveguide are relatively small.

7. Future Work

For the coaxial reflection method that was used here other models of the open-ended coaxial probe can be used (Pournaropoulos and Misra 1997, Bérubé *et al.*1996, Chen *et al.*2004 pp. 145-149) and other calibration procedures (Nyshadam *et al.* 1992).

Other methods must be investigated and implemented for partially filled waveguides as the work presented on [Catalá-Civera *et al.* 2003].

More experiments, more simulations and more data process have to be done on partially filled waveguides and an optimum algorithm to be found.

8. References

Agilent (2006). "Basics of Measuring the Dielectric Properties of Materials", *Application Note, Literature number 5989-2589 EN.*

Anderson, J.M. Sibbald, C.L. and Stuchly, S.S. (1994). "Dielectric measurements using a rational function model", *IEEE Transactions on Microwave Theory and Techniques*, **42** (2), 199-204.

Athey, T.W. Stuchly, M.A and Stuchly, S.S. (1982). "Measurement of radio-frequency permittivity of biological tissues with an open-ended coaxial line - Part I", *IEEE Transactions on Microwave Theory and Techniques*, **30** (1), 82-86.

Baker-Jarvis, J. (1990). "Transmission/Reflection and Short-Circuit Line Permittivity Measurements", NIST Technical Note, *National Institute of Standards and Technology, Bounder, Colorado 80303-3328.*

Bérubé, D. Ghannouchi, F.M. and Savard, P. (1996). "A comparative study of four open-ended coaxial probe models for permittivity measurements of lossy dielectric biological materials at microwave frequencies". *IEEE Transactions on Microwave Theory and Techniques*, **44** (10), 1928-1934.

Brady, M.M. Symons, S.A. and Stuchly, S.S. (1981). "Dielectric behavior of selected animal tissues *in vitro* at frequencies from 2 to 4 GHz", *IEEE Transactions on Biomedical Engineering*, **28** (3), 305-307.

Burdette, E.C. Cain, F.L. and Seals, J (1980). "*In vivo* probe measurement technique for determining dielectric properties at VHF through microwave frequencies", *IEEE Transactions on Microwave Theory and Techniques*, **28** (4), 414-427.

Catalá-Civera, J.M. Canós, A.J. Peñaranda-Foix, F.L. de los Reyes Davó, E. (2003). "Accurate determination of the complex permittivity of materials with transmission reflection measurements in partially filled rectangular waveguides", *IEEE Transactions on Microwave Theory and Techniques*, **51** (1), 16-24.

Chabbra, M. Fan, S.Q. and Misra, D. (1989). "A study on the open-ended coaxial line method for measuring the permittivity of materials at microwave frequencies", *6th IEEE Instrumentation and Measurement Technology Conference*, 541-545.

Chen, L.F. Ong, C.K. Neo, C.P. Varadan, V.V. and Varadan, V.K. (2004). *"Microwave Electronics Measurement and Materials Characterization"*, John Wiley & Sons Ltd, England.

Collin, R.E. (2001). *"Foundations for Microwave Engineering"*, 2nd edition, IEEE Press Series on Electromagnetic Wave Theory, The Institute of Electrical and Electronics Engineers, Inc, New York, John Wiley & Sons, Inc, New Jersey.

Debye, P. (1929). "Polar Molecules", *Chemical Catalog Company*, New York.

Deschamps, A. (1972). "Impedance of an antenna in a conducting medium", *IEEE Transactions on Antennas and Propagation*, **10** (5), 648-650.

Engen, C.F. and Hoer, C.A. (1979). "'Thru-Reflect-Line': An improved technique for calibrating the dual six-port automatic network analyzer", *IEEE Transactions on Microwave Theory and Techniques*, **27** (12), 987-993.

Fellner-Feldegg, H. (1969). "Measurement of dielectrics in the time domain", *The Journal of Physics Chemistry*. **73** (3), 616-623.

Gajda, G. and Stuchly, S.S. (1983). "An equivalent circuit of an open-ended coaxial line", *IEEE Transactions on Instrumentation and Measurement*, **32** (4), 506-508.

Ghannouchi, F.M. and Bosisio, R.G. (1989). "Measurement of microwave permittivity using six-port reflector with an open-ended coaxial line", *IEEE Transactions on Instrumentation and Measurement*, **38** (2), 505-508.

Grant, J.P. Clarke, R.N. Symm, G.T. and Spyrou, N.M. (1989). "A critical study of the open-ended coaxial line sensor technique for RF and microwave complex permittivity measurements", *Journal of Physics E: Scientific Instruments*, **22** (9), 757-770.

Jiles, D. (1994). *"Introduction to the Electronic Properties of Materials"*, Chapman & Hall, London.

Kaatze, U. (1989). "Complex permittivity of water as a function of frequency and temperature", *Journal of Chemical and Engineering Data*, **34** (4), 371-374.

Kittel, C. (1997). *"Introduction to Solid State Physics"* 7th edition, John Wiley & Sons, New York.

Knott, E.F. Shaeffer, J.F. Tuley, M.T. (2004). *"Radar Cross Section"*, 2nd edition, SciTech Publishing, Raleigh.

Larsson, C. Sjöberg, D. Elmkvist, L. (2011). "Waveguide Measurements of the permittivity and permeability at temperatures of up to 1000 ^{o}C", *IEEE Transactions on Instrumentation and Measurement*, **60** (8), 2872-2880.

Li, C.C. and Chen, K.M. (1995). "Determination of electromagnetic properties of materials using flanged open-ended coaxial probe-full wave analysis", *IEEE Transactions on Instrumentation and Measurement*, **44** (1), 19-27.

Marsland, T.P. and Evans, S. (1987). "Dielectric measurements with an open-ended coaxial probe", *IEE Proceedings*, **134** (4), 341-349.

Misra, D.K. (1987). "A quasi-static analysis of open-ended coaxial lines", *IEEE Transactions on Microwave Theory and Techniques*, **35** (10), 925-928.

Montrose, M.I. (1999). "*EMC and the Printed Circuit Board: Design, Theory, and Layout made Simple*", IEEE Press, The Institute of Electrical and Electronics Engineers, Inc, New York.

Nicolson, A.M. and Ross, G.F. (1970). "Measurement of the intrinsic properties of materials by time domain techniques", *IEEE Transactions on Instrumentation and Measurement*, **19** (4), 337-382

Nyfors, E. and Vainikainen, P. (1989). *"Industrial Microwave Sensors"*, Artech House, Norwood.

Nyshadam, A. Sibbald, C.L. and Stuchly, S. (1992). "Permittivity Measurements Using Open-Ended Sensors and Reference Liquid Calibration-An Uncertainty Analysis", *IEEE Transactions on Microwave Theory and Techniques*, **40** (2), 305-314.

Pournaropoulos, C.L. and Misra, D.K. (1997). "The coaxial aperture electromagnetic sensor and its application in material characterization", *Measurement Science and Technology*, **8** (11), 1191-1202.

Ramo, S. Whinnery, J.R. and Van Duzer, T. (1994). *"Fields and Waves in Communication Electronics"*, 3rd edition, John Wiley & Sons, New York.

Robert, P. (1988). *"Electrical and Magnetic Properties of Materials"*, Artech House, Norwood.

Sjöberg, D. and Larsson, C. (2011). "Cramér-Rao bounds for determination of permittivity and permeability in slabs", *IEEE Transactions on Microwave Theory and Techniques*, **59** (11), 2970-2977.

Solymar, L. and Walsh, D. (1998). "*Electrical Properties of Materials*", 6th edition, Oxford University Press, Oxford.

Staebell, K.F. and Misra, D. (1990). "An experimental technique for in vivo permittivity measurement of materials at microwave frequencies", *IEEE Transactions on Microwave Theory and Techniques*, **38** (3), 337-339.'

Stuchly, M.A. Athey, T.W. Samaras, C.M. and Taylor, G.E. (1982). "Measurement af radio frequency permittivity of biological tissues with an open-ended coaxial line: Part II - experimental results", *IEEE Transactions on Microwave Theory and Techniques*, **30** (1), 87-91.

Stuchly, S.S. Sibbald, C.L. and Anderson, J.M. (1994). "A new admittance model for open-ended waveguides" *IEEE Transactions on Microwave Theory and Techniques*, **42** (2), 192-198.

Stuchly, M.A. and Stuchly, S.S. (1980). "Coaxial line reflection methods for measuring dielectric properties of biological substances at radio and microwave frequencies - a review", *IEEE Transactions on Instrumentations and Measurement*, **29** (3), 176-183.

Suggett, A. Mackness, P.A Tait, M.J. Loeb,H.W. and Young, G.M. (1970). "Dielectric relaxation studies by time domain spectroscopy", *Nature* (228), 456-457.

Thuery, J. (1992). "*Microwaves: Industrial, Scientific and Medical Applications*", Artech House, Boston.

Von Hippel, A.R. (1995a). "*Dielectrics and Waves*", Artech House, Boston.

Von Hippel, A.R. (1995b). "*Dielectric Materials and Applications*", Artech House, Boston.

Waser, R. (2003). "*Nanoelectronics and Information Technology: Advanced Electronic Materials and Novel Devices*", Wiley-VCH, Cambridge.

Weir, W.B. (1974). "Automatic measurement of complex dielectric constant and permeability at microwave frequencies", *Proceedings of the IEEE*, **62** (1), 33-36.

Zoughi, R. (2000). "*Microwave Non-Destructive Testing and Evaluation*", Kluwer Academic Publishers, Dordrecht, Netherlands.